

# Data Analysis of three parameter models of deceleration parameter in FRW Universe

Amine Bouali,<sup>1,\*</sup> Himanshu Chaudhary,<sup>2,3,†</sup> Ujjal Debnath,<sup>4,‡</sup> Alok Sardar,<sup>4,§</sup> and G.Mustafa<sup>5,¶</sup>

<sup>1</sup>*Laboratory of Physics of Matter and Radiation,  
Mohammed I University, BP 717, Oujda, Morocco.*

<sup>2</sup>*Department of Applied Mathematics, Delhi Technological University, Delhi-110042, India,*

<sup>3</sup>*Department of Mathematics, Shyamla College, University of Delhi, Delhi-110032, India.*

<sup>4</sup>*Department of Mathematics, Indian Institute of Engineering Science and Technology, Shibpur, Howrah-711 103, India.*

<sup>5</sup>*Department of Physics, Zhejiang Normal University, Jinhua 321004, People's Republic of China,*

Constraining the dark energy deceleration parameter is one of the fascinating topics in the recent cosmological paradigm. This work aims to reconstruct the dark energy using parametrization of the deceleration parameter in a flat FRW universe filled with radiation, dark energy, and pressureless dark matter. Thus, we have considered four well-motivated parameterizations of  $q(z)$ , which can provide the evolution scenario from the deceleration to acceleration phase of the Universe. We have evaluated the expression of the corresponding Hubble parameter of each parametrization by imposing it into the Friedmann equation. We have constrained the model parameter through  $H(z)$ , Pantheon, and baryons acoustic oscillation (BOA) data. Next, we have estimated the best-fit values of the model parameters by using Monte Carlo Markov Chain (MCMC) technique and implementing  $H(z)$ + BAO+SNe-Ia dataset. Then we analyzed the cosmographic parameter, such as deceleration, jerk, and snap parameters, graphically by employing the best-fit values of the model parameter. Moreover, we have analyzed statefinder and  $Om$  diagnostics parameters for each scenario to discriminate various dark energy models. Using the information criteria, the viability of the models have examined. In the end, we have analogized our outcomes with the standard  $\Lambda$ CDM model to examine the viability of our models.

## I. INTRODUCTION

The confirmation of the cosmic accelerated expansion of the Universe through different surveys [1–3], opened an emerging field of study in modern cosmology. To disclose the physical mechanism behind the such accelerated expansion is a challenging task for modern researchers. In light of this, several cosmological models have been implemented to alleviate this phenomenon based mainly on two different approaches. The first approach is the modification of the gravitational part of the Einstein field equation-so called modified gravity [4, 5], and the other is the existence of an exotic fluid having positive energy density and negative pressure, named dark energy (DE). This work will mainly concentrate on the second approach and suppose that the DE is responsible for the universe's accelerated expansion [6–8]. It is also interesting to note that DE violates strong energy conditions. This violation of energy generates anti-gravitational effects for which the transition from deceleration to acceleration takes place [9]. So far, numerous DE models have been suggested to describe the present-day cosmic accelerated expansion [10–14]. Among them, the  $\Lambda$ CDM ( $\Lambda$ -cold dark matter) model is considered as simplest and widely accepted DE model. Despite its success, it suffers

from some other problems, namely *coincidence* problem, *fine-tuning* problem, and *age* problem [13, 15, 16]. To solve this issue, it is quite natural for physicists to figure out another alternative DE model that can describe the present status of the Universe. The scalar field models, like quintessence, phantom, k-essence, and so on, contribute to the understanding of the origins and nature of DE. Despite these designs of dark energy, cosmic accelerated expansion is still a problem in physics today.

Several theoretical approaches have been developed to describe the cosmic accelerated expansion phenomenon, but none of these is known as the appropriate one. The most recent direction to explore the accelerating Universe at the phenomenological level is the DE parametrization of the equation of state parameter. The main idea in this approach is to consider a specific evolution scenario instead of considering any DE model a priori and then determine the nature of the exotic component that is triggering cosmic acceleration. It is known as the model-independent approach, which depends on estimating model parameters from existing observational datasets. But such an approach has some drawbacks: (i) most of the parametrization suffers from divergence problem, (ii) the parametrization technique would have missed subtle results about the true nature of dark energy due to the assumed parametric form. Various studies have been executed to describe the cosmic acceleration of the Universe through viable parametrization of EOS (see Refs.[17–19]). Inspired by the parametrization of EOS, the parametrization of the deceleration parameter has been implemented and

\* [a1.bouali@ump.ac.ma](mailto:a1.bouali@ump.ac.ma)

† [himanshuch1729@gmail.com](mailto:himanshuch1729@gmail.com)

‡ [ujjaldebnath@gmail.com](mailto:ujjaldebnath@gmail.com)

§ [alokmath94@gmail.com](mailto:alokmath94@gmail.com)

¶ [gmustafa3828@gmail.com](mailto:gmustafa3828@gmail.com)

studied extensively in the literature. Since the Universe evolves from earlier deceleration to late time acceleration. For this reason, any cosmological model should have a transition from deceleration phase to acceleration phase of expansion to explain the whole evolution of the Universe. Thus, the deceleration parameter plays a crucial role which is defined by  $q = -\frac{\dot{a}\ddot{a}}{\dot{a}^2}$ , where  $a(t)$  is the usual scale factor. The sign of  $q$  decides whether the Universe is accelerating i.s. ( $q < 0$ ) or decelerating i.s.  $q > 0$ . Recently, several theoretical models have been developed to analyze the entire evolutionary history of the Universe through parametrization of  $q(z)$  as a function of scale factor ( $a(t)$ ) or time ( $t$ ) or redshift ( $z$ ) [20–34]. The advantage of the parametrization of deceleration parameter is that it can provide finite results without considering any particular gravitational theory. However, such approaches also have disadvantages similar to the parametrization of EOS. Since we do not yet have any concrete and satisfactory theoretical model of the Universe which can describe the whole evolutionary history of the Universe. So, the idea of adopting a parametric approach may be a preliminary step towards the expansion history of the Universe.

Recently, Mamon et al. [35] studied a special form of deceleration parameter and obtained the best-fit values using  $\chi^2$  minimization technique with available observational data. They also analyzed the evolution of the jerk parameter for the considered parametrized model. Gadbali, Mandal, and Sahoo [32] have explored a specific parametrization of deceleration parameter in the context of  $f(Q)$  gravity theory and constrained the model parameter by using Bayesian analysis with observational data. Motivated by the above work, we explored four suitable parametrizations of deceleration parameter to determine the best viable model compared to  $\Lambda$ CDM (see Ref. [36]). The present work is indeed an extension of our previous work. Here, we have assumed three well-motivated parametrizations (model 1-model3) of deceleration parameter containing three unknown parameters. We also introduced a new parametrization of the deceleration parameter, containing three unknown parameters. This work mainly focuses on constraining the model parameters using various observational datasets. In particular, we have chosen to use  $H(z)$  dataset consisting of 57 measurements, Pantheon dataset consisting of 1048 measurements, and 17 uncorrelated BAO measurements to get the best-fit values of the model parameters. We adopt Monte-Carlo Markov Chain (MCMC) analysis to fix the model parameters on the recently released data. We perform observational data analysis by  $\chi^2$ -minimization technique on the view of  $H(z)$ +SNIa+BAO dataset. This analysis provides us the bounds of arbitrary parameters  $q_0$ ,  $q_1$ , and  $q_2$  within  $1\sigma$ ,  $2\sigma$  confidence levels. In the end, we performed a graphical analysis of cosmographic parameters like deceleration, jerk, and snap parameters for all models. In addition to this, we have analyzed  $r - s$ ,  $q - r$  planes,

and  $Om$  diagnostics parameters for all the considered models.

The paper is structured as follows: section **II** is assigned for the basic equations for the FRW universe. In section **III**, we have adopted four parametrizations (model 1-model 3) and a new parametrization of the deceleration parameter. Then we obtained the Hubble solution for each parametrization. In section **IV**, the model parameters have been constrained using various datasets and place the best-fit values of the model parameters by implementing the MCMC method with observation data. In section **V**, we perform a cosmographic survey. The  $r - s$ ,  $q - r$  planes and  $Om$  diagnostic parameter is also addressed in section **VI** & **VII**. In section **VIII**, we present the information criteria for our models. In section **IX**, we have reported our conclusions based on the findings of our work.

## II. BASIC EQUATIONS OF FRW MODEL

The line element of the spatially flat Friedmann-Lemaître-Robertson-Walker (FLRW) universe is assumed as

$$ds^2 = -dt^2 + a^2(t) [dr^2 + r^2 (d\theta^2 + \sin^2\theta d\phi^2)] \quad (1)$$

with  $a(t)$  as the scale factor, as usual. The Friedmann equations are taken as

$$H^2 = \frac{8\pi G}{3} \rho \quad (2)$$

and

$$\dot{H} = -4\pi G(\rho + p) \quad (3)$$

here,  $H = \dot{a}/a$  is the Hubble parameter. We suppose that the universe is composed of radiation, dark matter (DM), and dark energy (DE). Then total energy density  $\rho$  and total pressure  $p$  becomes  $\rho = \rho_r + \rho_m + \rho_d$  and  $p = p_r + p_m + p_d$ . Now we consider that the radiation, DM, and DE are separately conserved. Thus, one can write

$$\dot{\rho}_r + 3H(\rho_r + p_r) = 0, \quad (4)$$

$$\dot{\rho}_m + 3H(\rho_m + p_m) = 0 \quad (5)$$

and

$$\dot{\rho}_d + 3H(\rho_d + p_d) = 0 \quad (6)$$

For radiation,  $p_r = \frac{1}{3}\rho_r$ , then from equation (4) we have  $\rho_r = \rho_{r0}a^{-4}$ . If we assume pressure-less DM (i.e.,  $p_m = 0$ ), from equation (5) we get  $\rho_m = \rho_{m0}a^{-3}$ .

Now, the deceleration parameter can be written as

$$q = -1 - \frac{\dot{H}}{H^2} \quad (7)$$

So the corresponding deceleration parameter for DE has the expression [36, 37]

$$q_d = -1 - \frac{\dot{H}_d}{H_d^2} \quad (8)$$

where  $H_d$  is the Hubble rate corresponding to dark energy. So from equations (2) and (3), we can write

$$H_d^2 = \frac{8\pi G}{3} \rho_d \quad (9)$$

and

$$\dot{H}_d = -4\pi G(\rho_d + p_d) \quad (10)$$

Using equations (9), (10) and (6), the fluid energy density yields

$$\rho_d = \rho_{d0} e^{\int \frac{2(1+q_d)}{1+z} dz} \quad (11)$$

where  $\rho_{d0}$  represents the present value of the density parameter, and  $z$  is the redshift parameter described as  $1+z = \frac{1}{a}$  (presently,  $a_0 = 1$ ).

Defining the dimensionless density parameters as  $\Omega_{r0} = \frac{8\pi G \rho_{r0}}{3H_0^2}$ ,  $\Omega_{m0} = \frac{8\pi G \rho_{m0}}{3H_0^2}$  and  $\Omega_{d0} = \frac{8\pi G \rho_{d0}}{3H_0^2}$ , then from equation (2), we have the Hubble parameter as:

$$H^2(z) = H_0^2 [\Omega_{r0}(1+z)^4 + \Omega_{m0}(1+z)^3 + (1-\Omega_{r0}-\Omega_{m0}) e^{\int \frac{2(1+q_d)}{1+z} dz}] \quad (12)$$

### III. PARAMETERIZED DECELERATION PARAMETER

In this section, we consider some parameterized deceleration parameter analogs of some well-established parametric models of the equation of state parameter and calculated the corresponding Hubble parameter in terms of redshift  $z$ .

#### A. Model 1

The Alam-Sahni-Saini-Starobinsky (ASSS) model for parameterized equation of state parameter has been studied in [38, 39]. The equivalent ASSS type parametrization of deceleration parameter has been introduced in [40, 41] and is given by

$$q_d(z) = -1 + \frac{q_1(1+z) + 2q_2(1+z)^2}{3[q_0 + q_1(1+z) + q_2(1+z)^2]} \quad (13)$$

with  $q_0$ ,  $q_1$  and  $q_2$  are constants. Then the energy density reads

$$\rho_d = \rho_{d0} \{q_0 + q_1(1+z) + q_2(1+z)^2\}^{2/3} \quad (14)$$

From equation (12), we obtain

$$H^2(z) = H_0^2 [\Omega_{r0}(1+z)^4 + \Omega_{m0}(1+z)^3 + (1-\Omega_{r0}-\Omega_{m0}) (q_0 + q_1(1+z) + q_2(1+z)^2)^{2/3}] \quad (15)$$

#### B. Model 2

The Pade-II model for parameterized equation of state parameter has been explored in [42–44]. The equivalent Pade-II type parametrization of deceleration parameter has been introduced in [40, 41] which is taken as

$$q_d(z) = \frac{q_0 + q_1 \log(1+z)}{1 + q_2 \log(1+z)} \quad (16)$$

where  $q_0$ ,  $q_1$  and  $q_2$  are constants. Then the energy density yields

$$\rho_d = \rho_{d0} (1+z)^{(q_1+q_2)} \{1 + q_2 \log(1+z)\}^{\frac{2(q_0 q_2 - q_1)}{q_2^2}} \quad (17)$$

From equation (12), we obtain

$$H^2(z) = H_0^2 [\Omega_{r0}(1+z)^4 + \Omega_{m0}(1+z)^3 + (1-\Omega_{r0}-\Omega_{m0}) (1+z)^{(q_1+q_2)} (1 + q_2 \log(1+z))^{\frac{2(q_0 q_2 - q_1)}{(q_2)^2}}] \quad (18)$$

#### C. Model 3

The Pade-I model for parameterized equation of state parameter has been investigated in [42–44]. The equivalent Pade-I type parametrization of deceleration parameter has been introduced in [40, 41], which takes the form:

$$q_d(z) = \frac{q_0 z + q_1(1+z)}{1 + q_2(1+z)} \quad (19)$$

where  $q_0$ ,  $q_1$  and  $q_2$  are constants. The energy density becomes

$$\rho_d = \rho_{d0} (1+z)^{2(1-q_0)} (1 + q_2 + q_2 z)^{\frac{2(q_0+q_1+q_0 q_2)}{q_2}} \quad (20)$$

From equation (12), we obtain

$$H^2(z) = H_0^2 [\Omega_{r0}(1+z)^4 + \Omega_{m0}(1+z)^3 + (1-\Omega_{r0}-\Omega_{m0}) (1+z)^{2(1-q_0)} (1 + q_2 + q_2 z)^{\frac{2(q_0+q_1+q_0 q_2)}{q_2}}] \quad (21)$$

## D. New Model

We propose a new model of deceleration parameter given as

$$q_d(z) = q_0 + \frac{2 + (1+z)^3}{q_1 + q_2(1+z)^3} \quad (22)$$

where  $q_0$  and  $q_1$  are constants. Thus, the energy density (11) reads

$$\rho_d = \rho_{d0} (1+z)^{3(1+q_0+\frac{2}{q_1})} [q_1 + q_2(1+z)^3]^{\frac{(q_1-2q_2)}{q_1q_2}} \quad (23)$$

From equation (12), we obtain

$$\begin{aligned} H^2(z) = & H_0^2 [\Omega_{r0}(1+z)^4 + \Omega_{m0}(1+z)^3 \\ & + (1 - \Omega_{r0} - \Omega_{m0}) (1+z)^{3(1+q_0+\frac{2}{q_1})} \\ & [q_1 + q_2(1+z)^3]^{\frac{(q_1-2q_2)}{q_1q_2}}] \end{aligned} \quad (24)$$

## IV. DATA DESCRIPTION WITH RESULTS

### A. Data description

Throughout this part, we will use three distinct observational datasets to limit our model parameters. We utilized the  $H(z)$  datasets of 57 measurements, the Pantheon dataset of 1048, 17 uncorrelated BAO measurements, and CMB Distant Prior to achieving the optimal value for the proposed model parameters. To construct the MCMC [45], we used the open-source tools Polychord [46] and GetDist [47]. The total  $\chi^2$  function of the combination  $H(z) +$  Pantheon + BAO + CMB and define as

$$\chi_{tot}^2 = \chi_{H(z)}^2 + \chi_{SN}^2 + \chi_{BAO}^2 + \chi_{CMB}^2. \quad (25)$$

#### 1. $H(z)$ Dataset

Numerous observational datasets must be used to achieve significant constraints on the model parameters. We employ the  $H(z)$  measurements in our investigation to constrain the model parameters. In general, the Hubble parameter can be determined either by estimating the BAO in the radial direction of galaxy clustering [48] or using the differential age technique, which also provides the redshift dependency of the Hubble parameter as

$$H(z) = -\frac{1}{1+z} \frac{dz}{dt}, \quad (26)$$

here  $dz/dt$  is computed using two moving galaxies in a proportionate manner. To estimate the model's parameters, the study takes into account 57 Hubble measurements, which are spans throughout the redshift range of

$0.07 \leq z \leq 2.42$ . To compare the model's theoretical predictions with observation, we use the chi-square function.

$$\chi_H^2 = \sum_{i=1}^{57} \frac{[H_{th}(z_i) - H_{obs}(z_i)]^2}{\sigma_{H(z_i)}^2}, \quad (27)$$

where  $H_{th}$  and  $H_{obs}$  denote the model prediction and observed value of Hubble rate, respectively. Also,  $\sigma_{H(z_i)}$  characterizes the standard error at the redshift  $z_i$ . The Hubble function numerical values for the appropriate redshifts are shown in [49].

### 2. Pantheon Dataset

The comic accelerated expansion is determined by measuring type Ia supernovae (SNIa). So far, SNIa has proven to be one of most robust successful methods for studying the nature of dark energy. In recent years, several supernova data sets have been established [50–54]. The Pantheon sample has lately been updated [55]. The former dataset contains 1048 spectroscopically verified SNIa spanning in the redshift range of  $0 < z < 2.3$ . SNIa are also astronomical objects that act as standard candles for determining relative distances. As a consequence, SN Ia samples are combined with the distance modulus  $\mu = m - M$ , where  $m$  indicates a certain object's apparent magnitude of a specific SNIa. The chi-square of the SNIa measurements is given by

$$\chi_{SN}^2 = \Delta\mu^T \cdot \mathbf{C}_{SN}^{-1} \cdot \Delta\mu. \quad (28)$$

$\mathbf{C}_{SN}$  is represented by a covariance matrix, and  $\Delta\mu = \mu_{obs} - \mu_{th}$ , where  $\mu_{obs}$  signifies the measured distance modulus of a certain SNIa, meanwhile the theoretical distance modulus is represented as  $\mu_{th}$ , and calculated as

$$\mu_{th}(z) = 5 \log_{10} \frac{D_L(z)}{(H_0/c)Mpc} + 25, \quad (29)$$

Here  $H_0$  signifies the current Hubble rate, and  $c$  reflects the speed of light. In a flat FLRW Universe, the luminosity distance,  $D_L$ , is given by:

$$D_L(z) = (1+z)H_0 \int_0^z \frac{dz'}{H(z')}. \quad (30)$$

Because we limit the model's free parameters at the same time, i.e., by using the Pantheon sample, and hence

$$\chi_{SN}^2 = \Delta\mu^T \times \mathbf{C}_{Pantheon}^{-1} \times \Delta\mu.$$

### 3. Uncorrelated Baryon Acoustic Oscillations (unCor BAO)

We picked 17 uncorrelated BAO (please see table 1 of this work [56]) measures from [57–68] the greatest BAO dataset of (333) measurements because considering the whole catalog of BAO might result in a very considerable inaccuracy because of data correlations; so we chose a representative subset to minimize errors. Transverse BAO experiments produce measurements of  $D_H(z)/r_d = c/H(z)r_d$  along with a co-moving angular diameter distance [69, 70].

$$D_M = \frac{c}{H_0} S_k \left( \int_0^z \frac{dz'}{E(z')} \right), \quad (31)$$

with

$$S_k(x) = \begin{cases} \frac{1}{\sqrt{\Omega_k}} \sinh(\sqrt{\Omega_k}x) & \text{if } \Omega_k > 0 \\ x & \text{if } \Omega_k = 0 \\ \frac{1}{\sqrt{-\Omega_k}} \sin(\sqrt{-\Omega_k}x) & \text{if } \Omega_k < 0. \end{cases} \quad (32)$$

Considering the angular diameter distance  $D_A = D_M/(1+z)$  and the  $D_V(z)/r_d$ . This corresponds to the combination of the BAO peaked coordinates and the sound horizon  $r_d$  at the drag epoch. Furthermore, we could immediately derive "line-of-sight" (or "radial") observations from the Hubble parameter.

$$D_V(z) \equiv [z D_H(z) D_M^2(z)]^{1/3}. \quad (33)$$

### 4. Cosmic Microwave Background

The CMB Distant Prior measurements are taken from Ref. [71]. Using distance priors, you can gain helpful information about the CMB power spectrum in two ways: the acoustic scale  $l_A$  represents the temperature power spectrum of the CMB in the transverse direction, and the "shift parameter"  $R$  affects the temperature spectrum of the CMB along the line-of-sight path to determine peak heights as follows:

$$l_A = (1+z_d) \frac{\pi D_A(z)}{r_s}, \quad (34)$$

$$R(z) = \frac{\sqrt{\Omega_m} H_0}{c} (1+z_d) D_A(z) \quad (35)$$

These are the observables that are reported [71]:  $R_z = 1.7502 \pm 0.0046$ ,  $l_A = 301.471 \pm 0.09$ ,  $n_s = 0.9649 \pm 0.0043$  and  $r_s$  is an independent parameter, with an associated covariance matrix (see Ref. [71]). The points represent the inflationary observables as well as the CMB epoch expansion rate. Besides the CMB points, we also

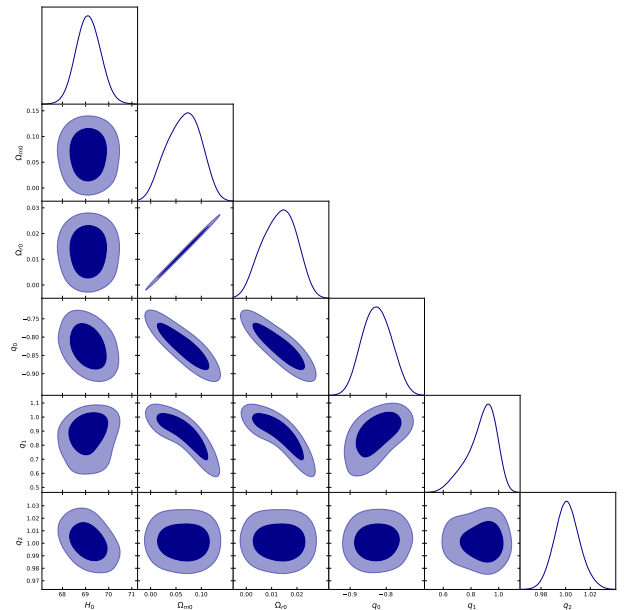


FIG. 1. Plot of MCMC confidence contours at  $1\sigma$  and  $2\sigma$  for Model 1.

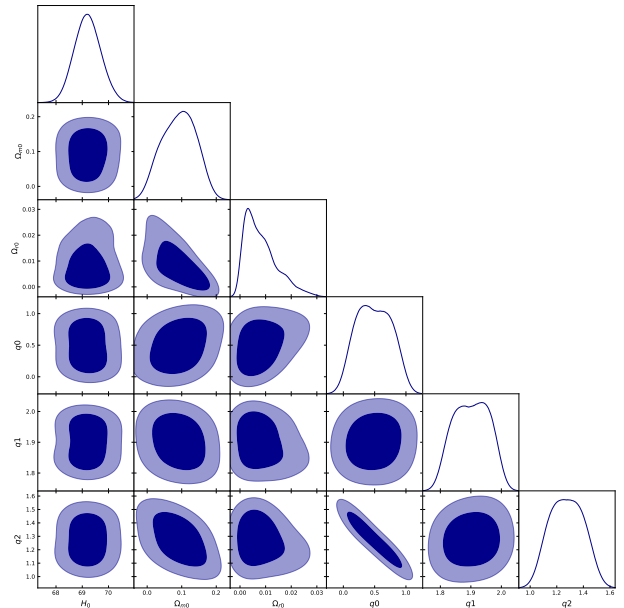


FIG. 2. Plot of MCMC confidence contours at  $1\sigma$  and  $2\sigma$  for Model 2.

consider other data from the late universe. The result is a successful test of the model in relation to the data.

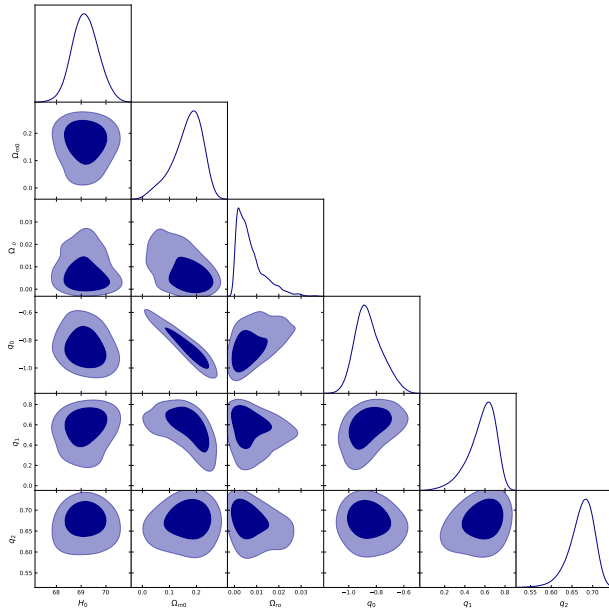


FIG. 3. Plot of MCMC confidence contours at  $1\sigma$  and  $2\sigma$  for Model 3.

MCMC Results		
Model	Parameters	Bestfit Value
Model 1	$H_0$	$69.121060^{+0.517902}_{-0.517902}$
	$\Omega_{m0}$	$0.065585^{+0.038524}_{-0.038524}$
	$\Omega_{r0}$	$0.013117^{+0.007705}_{-0.007705}$
	$q_0$	$-0.825763^{+0.041951}_{-0.041951}$
	$q_1$	$0.879053^{+0.111601}_{-0.111601}$
	$q_2$	$1.001254^{+0.010014}_{-0.010014}$
Model 2	$H_0$	$69.203662^{+0.529034}_{-0.529034}$
	$\Omega_{m0}$	$0.192287^{+0.058696}_{-0.058696}$
	$\Omega_{r0}$	$0.008128^{+0.006286}_{-0.006286}$
	$q_0$	$0.489155^{+0.311871}_{-0.311871}$
	$q_1$	$1.902027^{+0.066852}_{-0.066852}$
	$q_2$	$1.274424^{+0.143687}_{-0.143687}$
Model 3	$H_0$	$69.789290^{+0.469419}_{-0.649419}$
	$\Omega_m$	$0.205031^{+0.084481}_{-0.084481}$
	$\Omega_{r0}$	$0.00175^{+0.007645}_{-0.007645}$
	$q_0$	$-0.780911^{+0.060833}_{-0.060833}$
	$q_1$	$0.610530^{+0.067778}_{-0.067778}$
	$q_2$	$0.680228^{+0.285537}_{-0.285537}$
Model 4	$H_0$	$69.391442^{+0.478121}_{-0.478121}$
	$\Omega_{m0}$	$0.280604^{+0.006564}_{-0.006564}$
	$\Omega_{r0}$	$0.023950^{+0.017250}_{-0.017250}$
	$q_0$	$-2.975495^{+0.764170}_{-0.764170}$
	$q_1$	$1.000462^{+0.009284}_{-0.009284}$
	$q_2$	$0.646235^{+0.023499}_{-0.023499}$

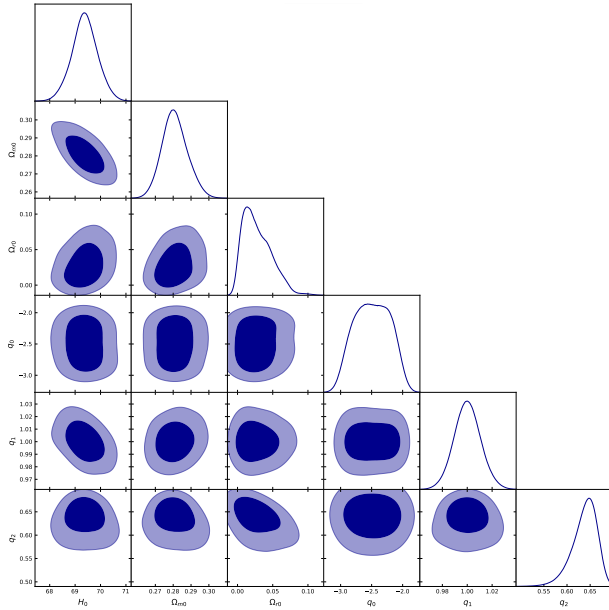


FIG. 4. Plot of MCMC confidence contours at  $1\sigma$  and  $2\sigma$  for Model 4.

## B. Observational, and theoretical comparisons of the Hubble functions

Following extracting the best-fit value of the free parameter of each Model, one could also contrast the model predictions against the observational data and also the  $\Lambda$ CDM model, correspondingly.

### 1. Comparison with the Hubble data points.

Each model has been compared to the 57 Hubble measurements,  $\Lambda$ CDM model, and  $1\sigma$  and  $2\sigma$  error bands. The comparison findings are shown in Figs. 5, 6, 7, 8. The Figure illustrates that each model accurately fits with the Hubble measurements.

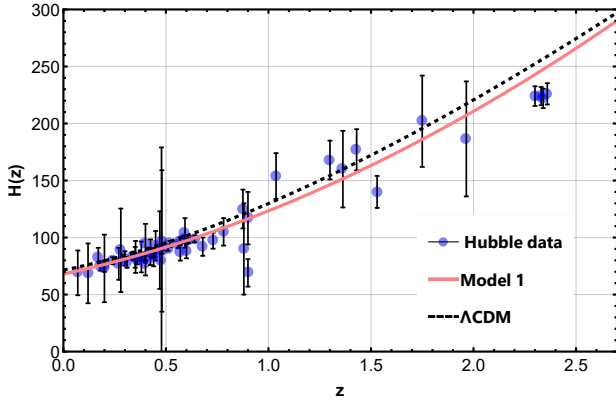


FIG. 5. Shows the plot of Hubble function  $H(z)$  for Model 1 (pink line),  $\Lambda$ CDM model (black dotted line) with  $\Omega_{m0} = 0.3$  and  $\Omega_{\Lambda} = 0.7$ , against Hubble measurements (blue dots) .

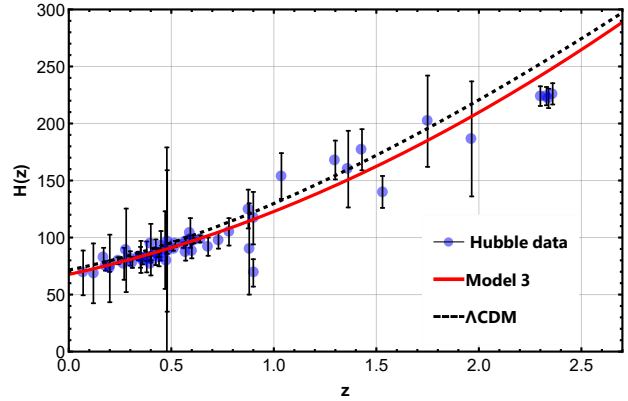


FIG. 7. Shows the plot of Hubble function  $H(z)$  for Model 3 (red line),  $\Lambda$ CDM model (black dotted line) with  $\Omega_{m0} = 0.3$  and  $\Omega_{\Lambda} = 0.7$ , against Hubble measurements (blue dots) .

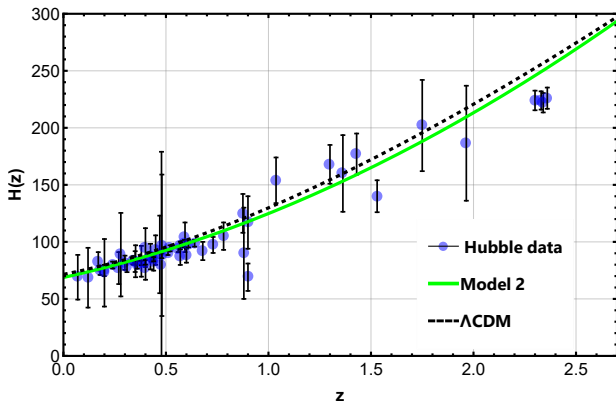


FIG. 6. Shows the plot of Hubble function  $H(z)$  for Model 2 (green line),  $\Lambda$ CDM model (black dotted line) with  $\Omega_{m0} = 0.3$  and  $\Omega_{\Lambda} = 0.7$ , against Hubble measurements (blue dots) .

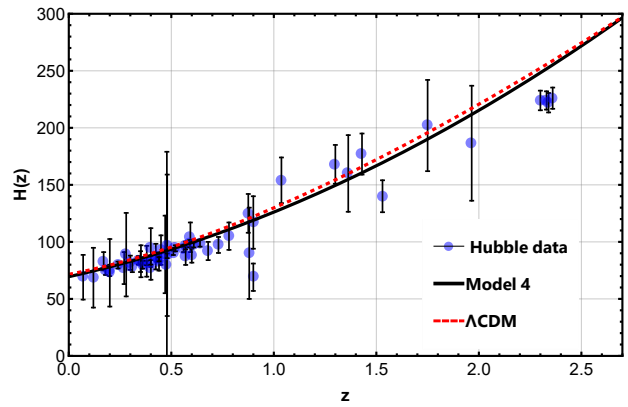


FIG. 8. Shows the plot of Hubble function  $H(z)$  for Model 4 (black line),  $\Lambda$ CDM model (red dotted line) with  $\Omega_{m0} = 0.3$  and  $\Omega_{\Lambda} = 0.7$ , against Hubble measurements (blue dots) .

## 2. Comparison with the Pantheon data.

Each model has been compared to the 1048 Pantheon dataset,  $\Lambda$ CDM model, and  $1\sigma$  and  $2\sigma$  error bands. The comparison findings are shown in Figs. 9, 10, 11, 12, One could see that each model matches the Pantheon dataset quite well.

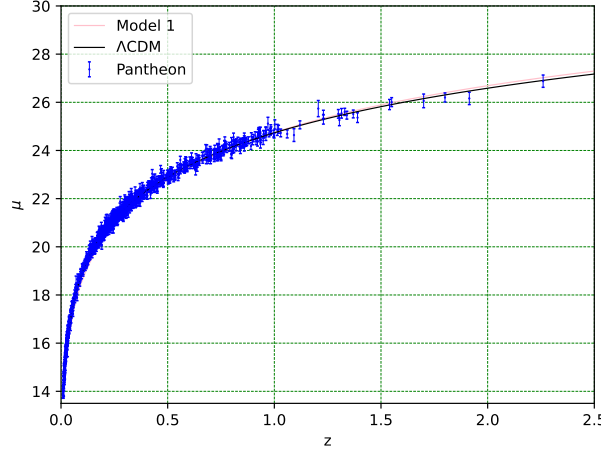


FIG. 9. Shows the plot of distance modulus  $\mu(z)$  for Model 1 (pink line),  $\Lambda$ CDM model (in black line) with  $\Omega_{m0} = 0.3$  and  $\Omega_{\Lambda} = 0.7$ , against type Ia supernova data (blue dots)

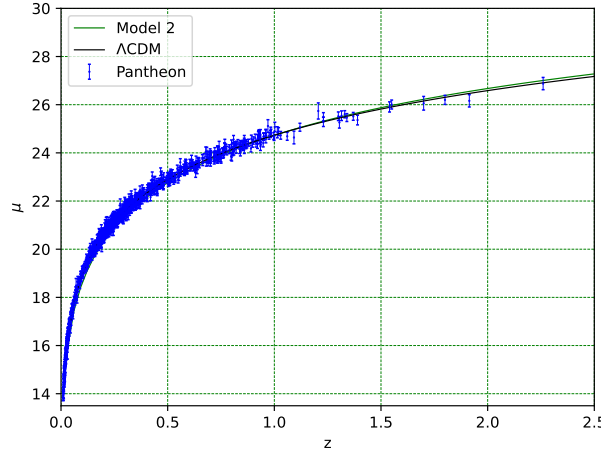


FIG. 10. Shows the plot of distance modulus  $\mu(z)$  of the model 2 (green line),  $\Lambda$ CDM model (black line) with  $\Omega_{m0} = 0.3$  and  $\Omega_{\Lambda} = 0.7$ , against type Ia supernova data (blue dots) .

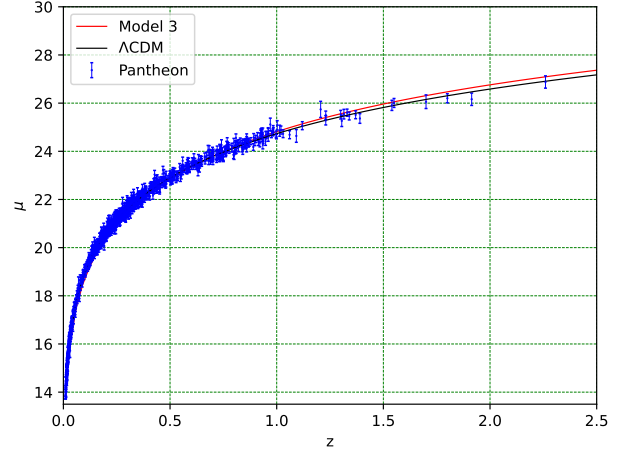


FIG. 11. Shows the plot of distance modulus  $\mu(z)$  of the model 3 (red line),  $\Lambda$ CDM model (black line) with  $\Omega_{m0} = 0.3$  and  $\Omega_{\Lambda} = 0.7$ , against type Ia supernova data (blue dots) .

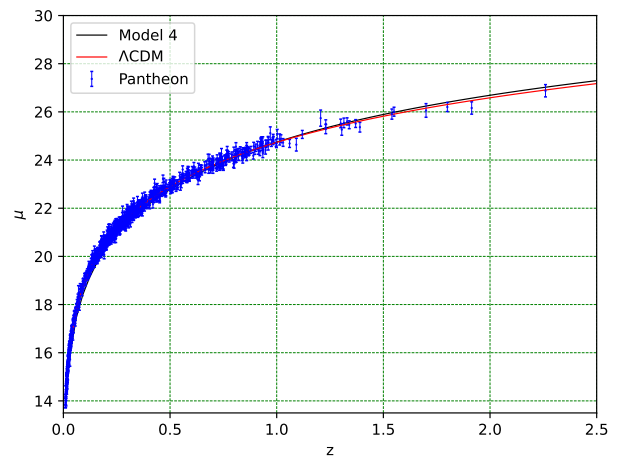


FIG. 12. Shows the plot of distance modulus  $\mu(z)$  of the model 4 (black line),  $\Lambda$ CDM model (black line) with  $\Omega_{m0} = 0.3$  and  $\Omega_{\Lambda} = 0.7$ , against type Ia supernova data (blue dots) .

### 3. Relative difference between Each Model and $\Lambda$ CDM.

Consequently, The relative difference between each model and the  $\Lambda$ CDM standard paradigm has been in Figs. 13, 14, 15, 16. At low redshift, each model behaves substantially identically; however, some distinctions between each model and  $\Lambda$ CDM paradigm emerge at high redshift.

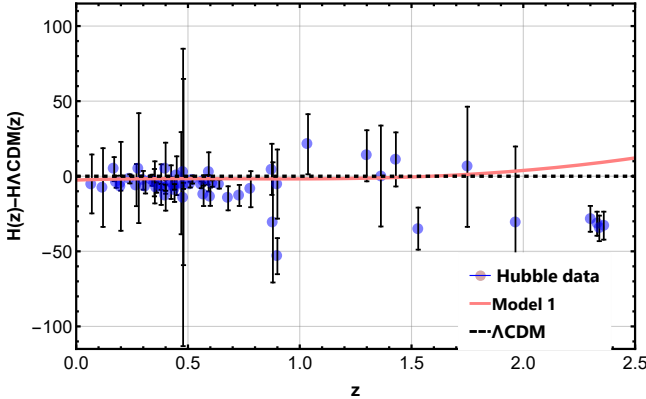


FIG. 13. Shows the Relative difference between Model 1 (pink line), the  $\Lambda$ CDM model (black dotted line) with  $\Omega_{m0} = 0.3$  and  $\Omega_{\Lambda} = 0.7$ , against the 57 Hubble measurements (blue dots), along with their corresponding error bars.

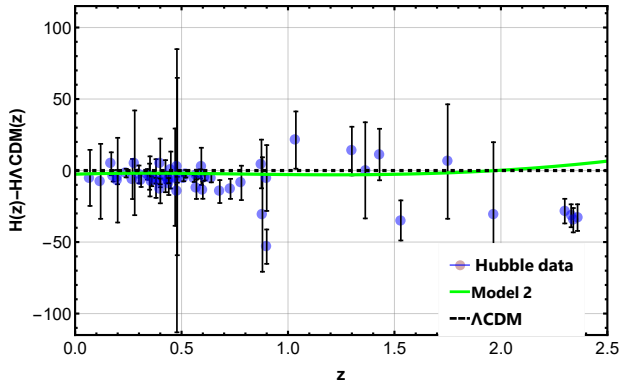


FIG. 14. Shows the Relative difference between Model 2 (Green line) and the  $\Lambda$ CDM model (black dotted line) with  $\Omega_{m0} = 0.3$  and  $\Omega_{\Lambda} = 0.7$ , against the 57 Hubble measurements (blue dots) along with their corresponding error bars.

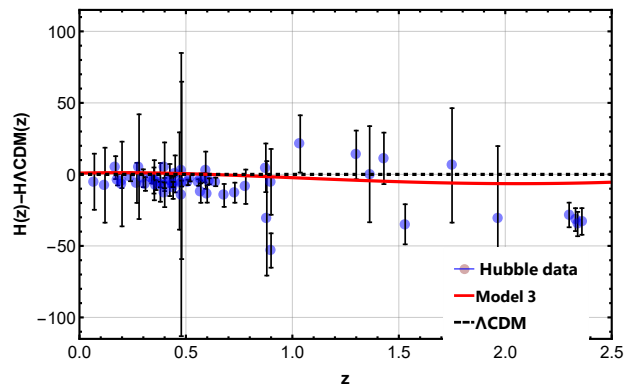


FIG. 15. Shows the Relative difference between Model 3 (red line), the  $\Lambda$ CDM model (black dotted line) with  $\Omega_{m0} = 0.3$  and  $\Omega_{\Lambda} = 0.7$ , against the 57 Hubble measurements (blue dots), along with their corresponding error bars.

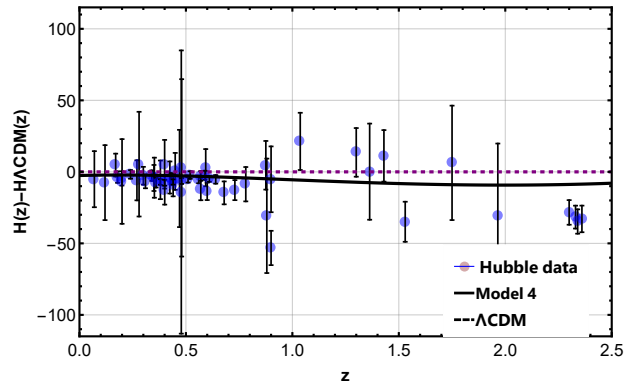


FIG. 16. Shows the Relative difference between Model 4 (black line) and the  $\Lambda$ CDM model (purple dotted line) with  $\Omega_{m0} = 0.3$  and  $\Omega_{\Lambda} = 0.7$ , against the 57 Hubble measurements (blue dots) along with their corresponding error bars.

## V. DYNAMICAL ANALYSIS OF THE MODEL

Our main focus in this work is to evaluate a cosmological model that can describe the universe's whole dynamics by examining its geometrical and physical parameters on large scale. This aim is to study the kinematic quantities, characterizing the cosmological behavior at both the early and late evolution of the universe. Now cosmological principle implies that the scale factor is an important ingredient that governs the universe. Therefore, it is reasonable to expand  $a(t)$  in Taylor series around the current time  $t_0$  gives

$$a(t) = a_0 \left[ 1 + \frac{(t-t_0)}{1!} \frac{da}{dt} \Big|_{t_0} + \frac{(t-t_0)^2}{2!} \frac{d^2a}{dt^2} \Big|_{t_0} + \frac{(t-t_0)^3}{3!} \frac{d^3a}{dt^3} \Big|_{t_0} + \frac{(t-t_0)^4}{4!} \frac{d^4a}{dt^4} \Big|_{t_0} + \mathcal{O}(t-t_0)^5 \right] \quad (36)$$

where  $a_0$  is the current value of the expansion factor evaluated at the present epoch  $t_0$ . In the above series expansion, the most important series terms define

$$H = \frac{1}{a} \frac{da}{dt}, \quad q = -\frac{1}{aH^2} \frac{d^2a}{dt^2}, \quad j = \frac{1}{aH^3} \frac{d^3a}{dt^3}, \quad s = \frac{1}{aH^4} \frac{d^4a}{dt^4}$$

which are usually known as the Hubble, deceleration, jerk, and snap parameters, respectively. These four geometrical quantities are sufficient to study the overall dynamics of the universe. We will discuss all these parameters for our model in detail in the following subsections.

### 1. DECELERATION, JERK, AND SNAP PARAMETER

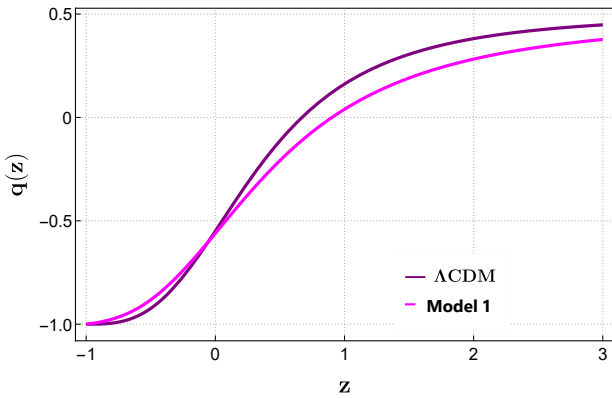


FIG. 17. Plot of deceleration parameter with respect to redshift.

*a. The deceleration parameter:* The deceleration parameter is one of the oldest and most influential cosmological parameter used to describe the evolution of the universe, which is defined by  $q = -\frac{\dot{a}\ddot{a}}{\dot{a}^2}$ , where  $a(t)$  is the

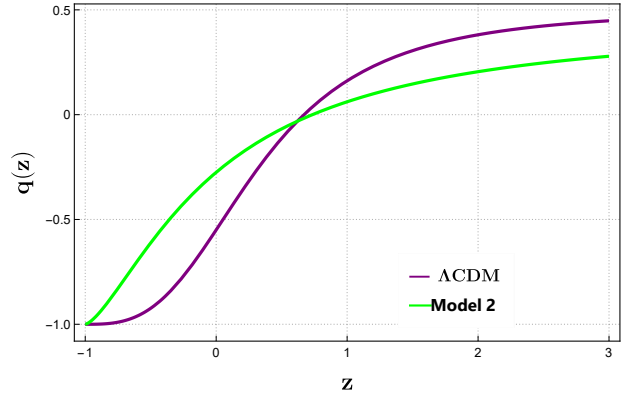


FIG. 18. Plot of deceleration parameter with respect to redshift.

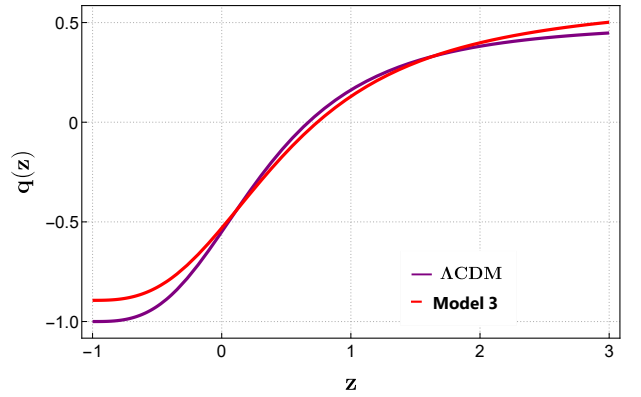


FIG. 19. Plot of deceleration parameter with respect to redshift.

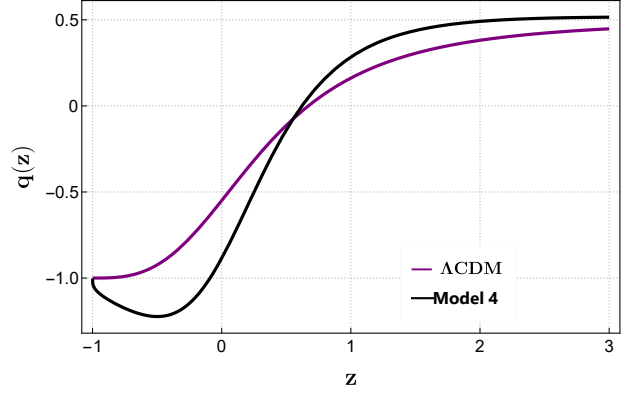


FIG. 20. Plot of deceleration parameter with respect to redshift.

usual scale factor. The sign of  $q$  decides whether the Universe is accelerating i.s. ( $q < 0$ ) or decelerating i.s.  $q > 0$ . In Figs. 17, 18, 19 and 20 the redshift dependency of the deceleration parameter  $q$  is displayed correspondingly for each model and  $\Lambda$ CDM models. Model 1 (M1) behavior is nearly identical to  $\Lambda$ CDM behavior at both high and low redshift; at low redshift, the M1 finishes in a de Sitter

phase, having  $q = -1$ . Model 2 (M2) has systematic differences at low and high redshift but also terminates in a de Sitter phase. At high redshift, Model 3 (M3) behaves very closely to  $\Lambda$ CDM, while at low redshift, a slower-accelerated evolution occurs, with  $q(-1) \approx -0.7$ . Lastly, Model 4 (M4) shows fascinating behavior at high and low redshifts. At low redshift, M4 exhibits super-accelerated evolution for some time but ends in the de Sitter phase.

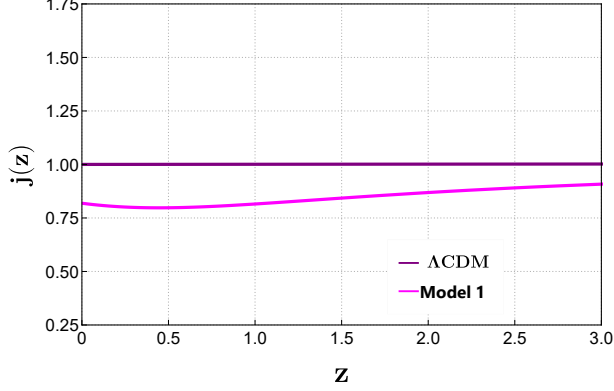


FIG. 21. Plot of jerk parameter with respect to redshift.

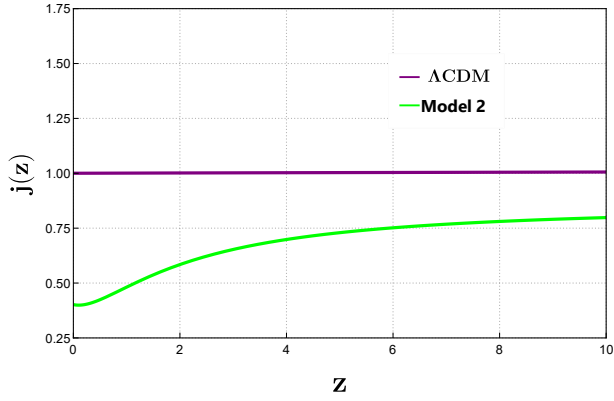


FIG. 22. Plot of jerk parameter with respect to redshift.

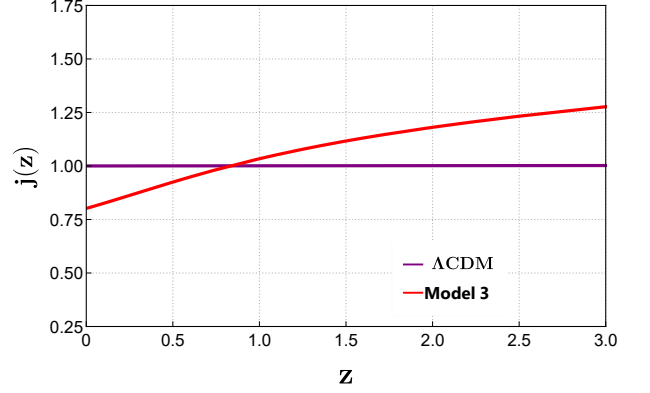


FIG. 23. Plot of jerk parameter with respect to redshift.

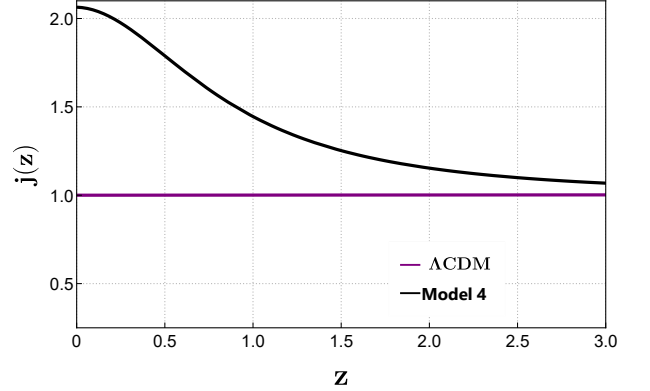


FIG. 24. Plot of jerk parameter with respect to redshift.

*b. The jerk parameter:* The jerk parameter as a function of  $q$  is given by  $j = \left[ (1+z) \frac{dq}{dz} + q(2q+1) \right]$ . The main feature of the jerk parameter is that for  $\Lambda$ CDM model,  $j = 1$  always. Therefore, any departure from  $j = 1$  would favor other dynamical DE models instead of  $\Lambda$ CDM [72]. The variability of the jerk parameter  $j(z)$  against redshift of each model with  $\Lambda$ CDM model shown in Figs. 21, 22, 23 and 24. A significant disparity exists among the quantitative values of  $j$  at high and low redshifts within every model. M1 has an approximate value of 0.79 at  $j(0)$ , M2 has an estimated value of 0.42, and M3 has an approximate value of 0.78 at  $j(0)$ . M4 has more than twice the numerical values of the  $\Lambda$ CDM model  $j(0) \approx 2.1$ . Identifying the current value of  $j$ 's provides an essential test.

*c. The snap parameter:* The snap parameter is the variation of of  $j$  which can be written as  $\mathcal{S} = \left[ -(1+z) \frac{d\dot{j}}{dz} - j(2+3q) \right]$ . This work also analyzed this geometrical parameter for each parametrization of  $q(z)$ . The progression of each model's snap parameter  $s(z)$  versus redshift could be noticed in Figs. 25, 26, 27 and 28. For both high and low redshift, every Model anticipates a big divergence between their and  $\Lambda$ CDM numerical values. At high redshifts, M1, M2, and M3 predict lower values than  $\Lambda$ CDM, but M4 predicts higher values than  $\Lambda$ CDM. Identifying the present value of  $s$ 's parameter is a critical test. M1 predicts  $s(0) \approx -0.1$ , M2 predicts  $s(0) \approx 0.9$ , M3 predicts  $s(0) \approx 0.7$ , and M4 estimates  $s(0) \approx 0.9$ .

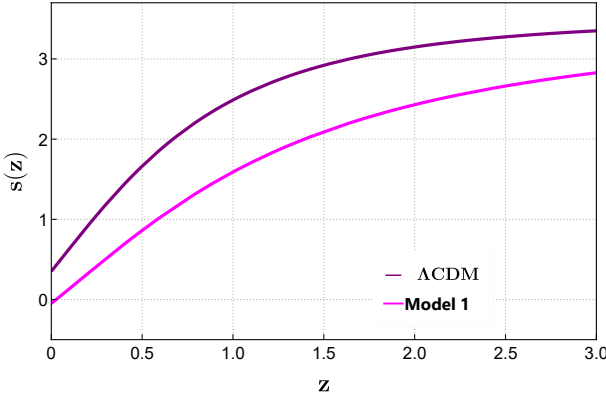


FIG. 25. Plot of snap parameter with respect to redshift.

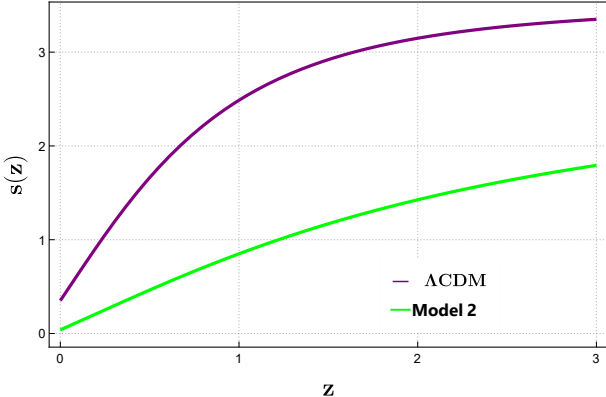


FIG. 26. Plot of snap parameter with respect to redshift.

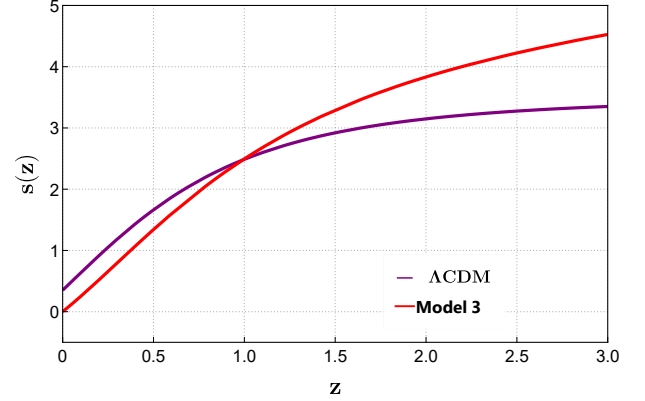


FIG. 27. Plot of snap parameter with respect to redshift.

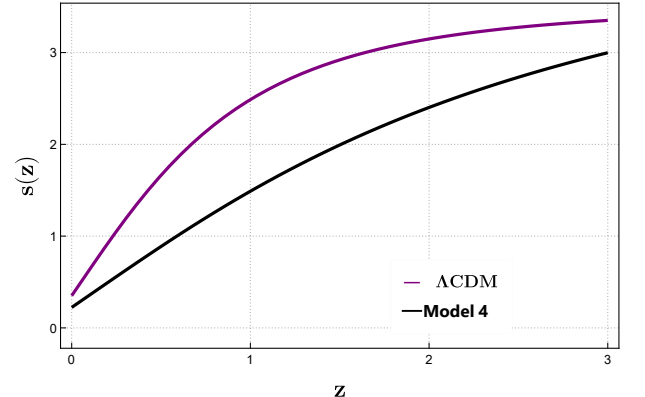


FIG. 28. Plot of snap parameter with respect to redshift.

## VI. STATEFINDER DIAGNOSTIC

It is a mechanism generally applied to explore different DE models and comprehend their nature through higher-order derivatives of the scale factor. The statefinder diagnostic pair [73–76]  $\{r, s\}$  is dimensionless, which can be used to analyze the cosmic features of DE independent of models and can be computed by the expressions [77, 78]

$$r = \left[ (1+z) \frac{dq}{dz} + q(2q+1) \right], \quad s = \frac{r-1}{3(q-\frac{1}{2})}, \quad (37)$$

where  $r$  and  $q$  are the usual *jerk* parameter and deceleration parameter respectively. Certain pairs commonly refer to the standard models of DE like  $\{r, s\} = \{1, 0\}$  shows  $\Lambda$ CDM model while  $\{r, s\} = \{1, 1\}$  corresponds to the standard cold dark matter model (SCDM) in FLRW universe. Moreover,  $(-\infty, \infty)$  indicates the Einstein static universe. In the  $r - s$  plane, one can obtain quintessence-like and phantom-like models of the DE for  $s > 0$  and  $s < 0$ , respectively. Also, the evolutionary process occurs (from phantom to quintessence) if the value deviates from the standard range  $r, s = 1, 0$ . The value  $\{q, r\} = \{-1, 1\}$  is associated with the  $\Lambda$ CDM model whereas  $\{q, r\} = \{0.5, 1\}$  gives SCDM model.

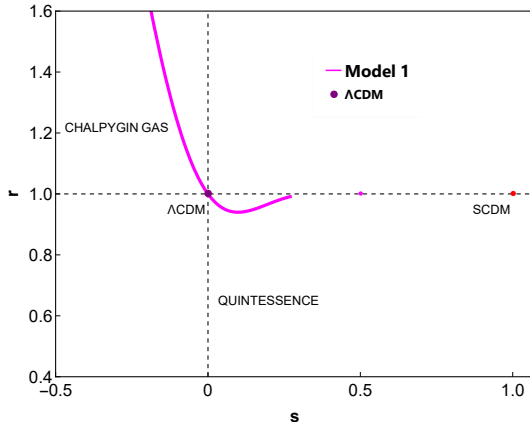


FIG. 29. Behavior of  $\{s, r\}$  profile of Model 1

a. *The  $\{s, r\}$  Parameter:* Figs. 29, 30, 31 and 32 shows the evolution of the model M1, M2, M3, and M4 of  $\{s, r\}$  parameter. At first, M1 takes values in the region  $r < 1, s > 0$  representing the quintessence domain, and afterward, by crossing fixed  $\{r, s\} = \{1, 0\}$ ,  $\Lambda$ CDM takes values in the region  $r < 1, s < 0$  Chaplygin gas region. Throughout evolution, M2 assumes values in the region  $r < 1, s > 0$  reflect the quintessence domain. The M3 begins with values in the region  $r > 1, s > 0$ , indicating the Chaplygin gas domain, and evolves to the quintessence region by traversing the intermediate  $\Lambda$ CDM fixed point  $\{1, 0\}$  during evolution. However, the  $\{s, r\}$  parameter of M4 exhibits identical behavior to M1.

b. *The  $\{q, r\}$  Parameter:* Figs. 33, 34, 35 and 36 of models M1, M2, M3, and M4 in  $\{q, r\}$  provide extra

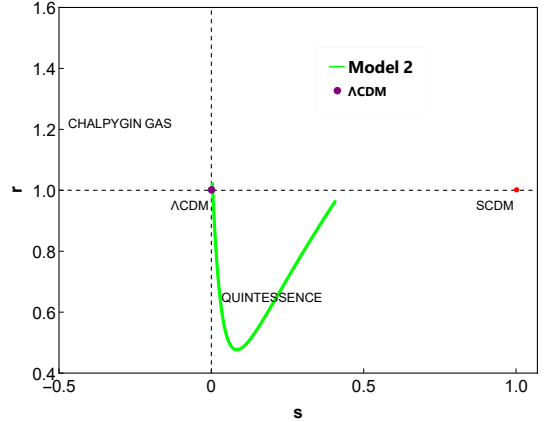


FIG. 30. Behavior of  $\{s, r\}$  profile of Model 2

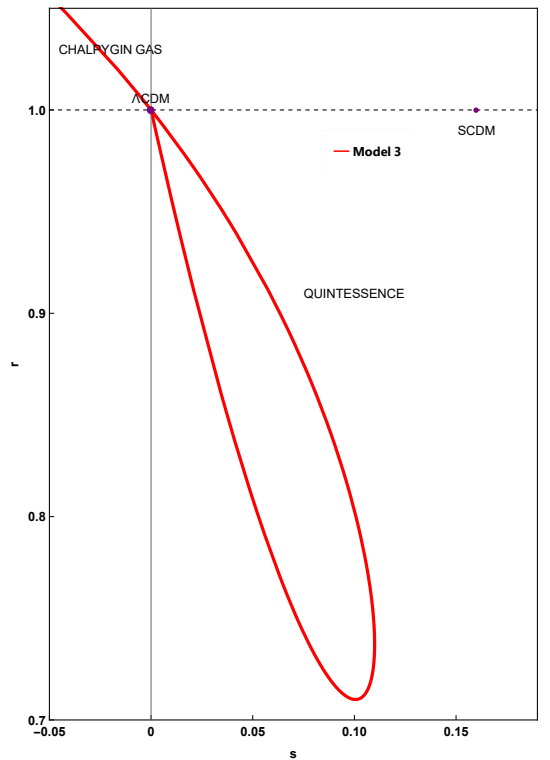
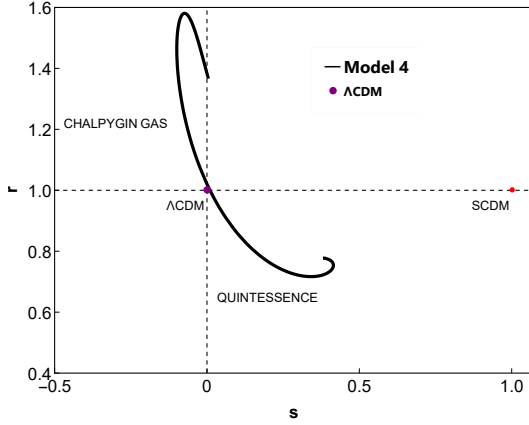
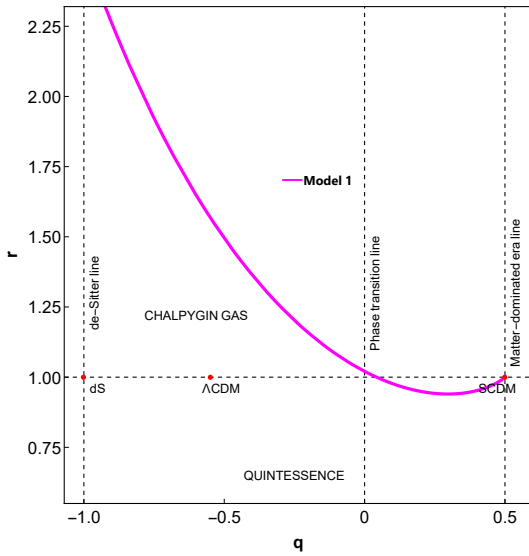
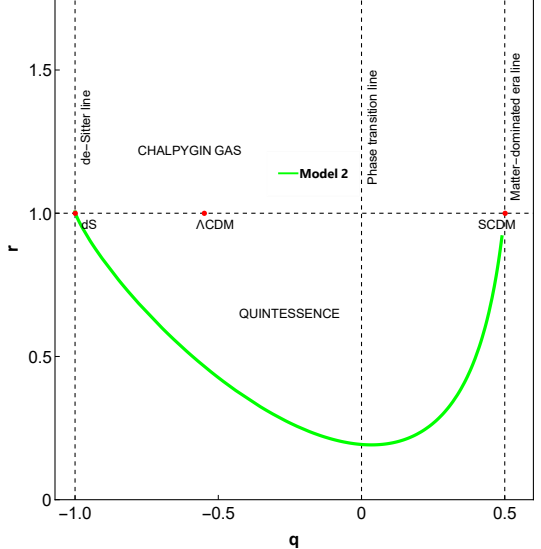
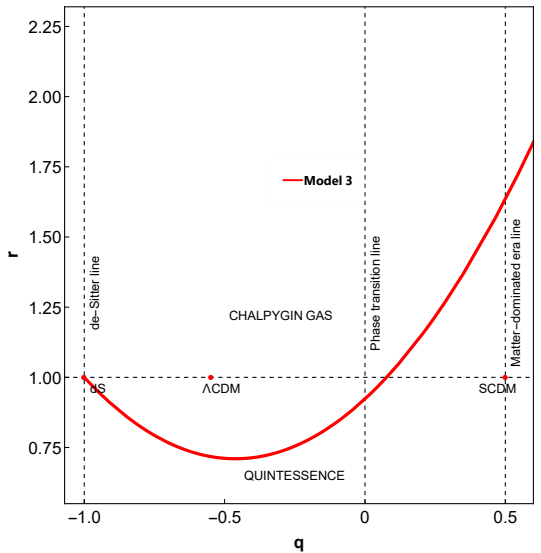


FIG. 31. Behavior of  $\{s, r\}$  profile of Model 3

information regarding M1, M2, M3, and M4. The evolution of this parameter of M1 indicates that at first M1 takes values in the range  $q > 0$  and  $r > 1$  indicating the quintessence region, then M1 takes values in the range  $q < 0$  and  $r < 1$  indicating the Chaplygin gas region, and eventually, it deviates towards the de Sitter point  $-1, 1$ . The  $\{q, r\}$  profile of M2 values remains in the quintessence area and terminates at the de Sitter point  $-1, 1$ . Whereas M3 acquires values in the range  $q > 0$  and  $r > 1$ , indicating the Chaplygin gas region, the trajectory of this Model's parameter eventually takes values in the range  $q < 0$  and  $r < 1$ , indicating the quintessence re-

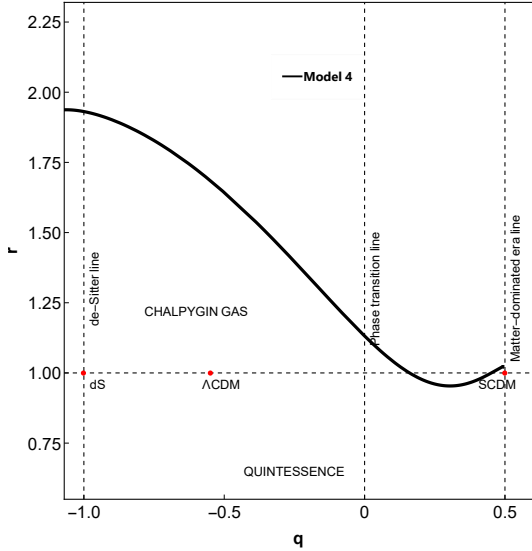
FIG. 32. Behavior of  $\{s, r\}$  profile of Model 4FIG. 33. Behavior of  $\{q, r\}$  profile of Model 1

gion and terminates at the de Sitter point  $\{-1, 1\}$ . M4's  $\{q, r\}$  parameter, on the other hands behave identically to M1.

FIG. 34. Behavior of  $\{q, r\}$  profile of Model 2FIG. 35. Behavior of  $\{q, r\}$  profile of Model 3

## VII. $Om$ DIAGNOSTIC

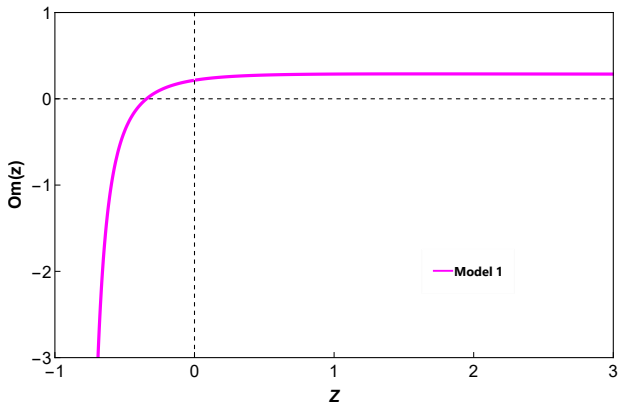
It refers to a geometrical formalism in which the Hubble parameter yields a null test for the  $\Lambda$ CDM model [79–82]. The  $Om$  diagnostic also efficiently differentiates several DE models from  $\Lambda$ CDM by the slope variation of  $Om(z)$ . A quintessence or phantom model can be acquired through either a positive or negative slope of the diagnostic parameter, respectively. Moreover, a constant slope with respect to redshift depicts a DE model corresponding to the cosmological constant. For a flat

FIG. 36. Behavior of  $\{q, r\}$  profile of Model 4

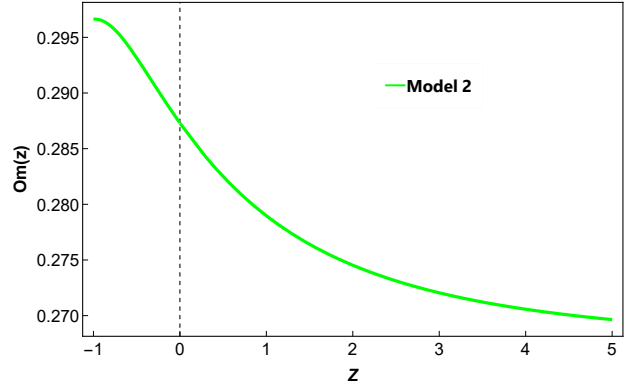
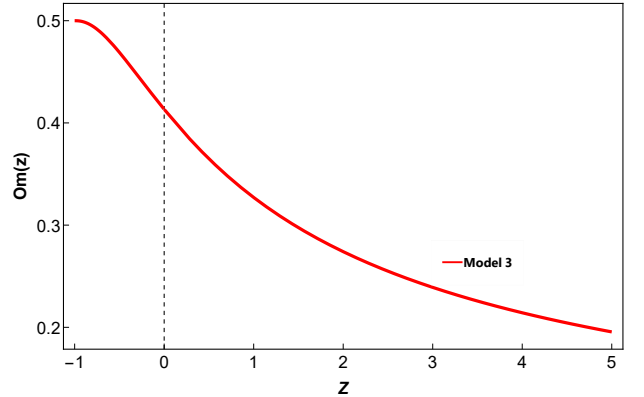
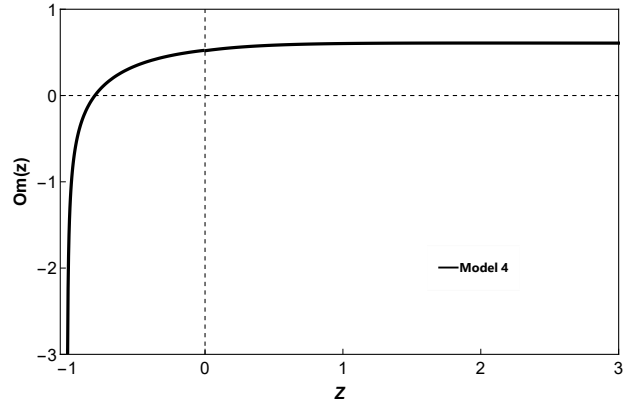
universe, one can define  $Om(z)$  as

$$Om(z) = \frac{\left(\frac{H(z)}{H_0}\right)^2 - 1}{(1+z)^3 - 1}. \quad (38)$$

Many authors have explored the behavior of various DE models from the viewpoint of statefinder and  $Om$  diagnostics parameter [83–86]. This diagnostic involves only the first-order temporal derivative compared to the statefinder diagnosis [72]. It can also be subjected to the Galileons models [87, 88].

FIG. 37. Evolution of  $Om$  profile of Model 1

a. *Om Diagnostic Parameter:* Each model's slope variation of  $Om(z)$  versus  $z$  is shown of each model in Figs. 37, 38, 39 and 40 respectively. Both models, M1 and M2, exhibit similar behavior at high redshift  $z > 0$ . Both models are in the quintessence region when redshift abruptly declines and becomes negative, meaning that both models reach the phantom region. Meanwhile, M2 is positive throughout high and low redshift, supporting

FIG. 38. Plot of  $Om$  profile of Model 2FIG. 39. Plot of  $Om$  profile of Model 3FIG. 40. Plot of  $Om$  profile of Model 4

a quintessence model. Ultimately, the M3 exhibits the same type of behavior.

## VIII. INFORMATION CRITERIA

To investigate the feasibility of any model, one needs first to comprehend the study of information criteria (IC). The Akaike Information Criteria (AIC) [89] is sim-

ply applied to all ICs. Because the AIC is an approximate minimization of the Kullback-Leibler information, it is an asymptotically unbiased estimator of Kullback-Leibler information. The AIC Gaussian estimator could be expressed as [90–93]  $AIC = -2 \ln(\mathcal{L}_{max}) + 2\kappa + \frac{2\kappa(\kappa+1)}{N-\kappa-1}$ , where  $\mathcal{L}_{max}$  is the maximum likelihood function,  $\kappa$  is the total number of free parameters of any model, and  $N$  is the total number of data points utilized. Because  $N \gg 1$ , is the assumption for the models, the aforementioned formula transforms to the original AIC like  $AIC = -2 \ln(\mathcal{L}_{max}) + 2\kappa$ . If a set of models is provided, the IC value deviations can be reduced to  $\Delta AIC = AIC_{model} - AIC_{min} = \Delta\chi^2_{min} + 2\Delta\kappa$ . The more favorable range of  $\Delta AIC$  are mentioned following  $\Delta AIC$  is  $(0, 2)$ . The low favorable range of  $\Delta AIC$  is  $(4, 7)$ , while  $\Delta AIC > 10$  provides less support model.

Model	$\chi^2_{min}$	$\chi^2_{red}$	$AIC$	$\Delta AIC$
$\Lambda$ CDM Model	1755.56	0.981	1762.32	0
Model 1	1751.10	0.963	1761.59	1.58
Model 2	1750.24	0.961	1761.59	0.73
Model 3	1750.02	0.972	1761.59	0.50
Model 4	1751.02	0.965	1761.59	1.50

TABLE I. Summary of the  $\chi^2_{min}$ ,  $\chi^2_{red}$ ,  $AIC$  and  $\Delta AIC$ .

## IX. DISCUSSIONS AND CONCLUSIONS

Herein, we have studied the accelerated expansion scenario in a flat FRW universe composed of DE, radiation, and DM. We have attempted to construct a viable dark energy model which can describe the whole evolutionary history of the Universe. For this purpose, we have taken parametrization of the deceleration parameter instead of assuming parameterization of EOS parameter. Here, we have considered three parametrizations (model 1–model 3) and also proposed one new parametrization of the deceleration parameter. The advantage of these parametrizations is that they can provide finite results without considering any particular gravitational theory and provide early deceleration and late-time acceleration. We have chosen  $q(z)$  containing only three parameters  $q_0$ ,  $q_1$  and  $q_2$ . Since the choice of  $q(z)$  is quite arbitrary, so one takes more than three terms for the parametrization of  $q(z)$ . But in that case, it may be difficult to constrain the parameters using existing observational data. A statistical analysis has been made to get the best-fit values of the model parameters by the MCMC method using  $H(z)$  datasets, Pantheon datasets and BAO datasets. We have analyzed the evolutionary trajectories of deceleration, jerk, and snap parameters by using the best-fit values of the model parameters. Moreover, the best-fit values of the model parameters obtained are used to plot the statefinder

and  $Om$  diagnostics. The information criteria have been employed to examine the models' viability. We examined all of the models and the  $\Lambda$ CDM model (the basic reference) to figure out which is more probable than the others. From Table: I

The results obtained by analyzing all the geometrical parameters are summarized as follows:

- The deceleration parameter for M1 behavior is nearly identical to  $\Lambda$ CDM behavior at both high and low redshift; at low redshift, the M1 finishes in a de Sitter phase. M2 has systematic differences at low and high redshift but also terminates in a de Sitter phase. At high redshift, M3 behaves very closely to  $\Lambda$ CDM, while at low redshift, a slower-accelerated evolution occurs, with  $q(-1) \approx -0.7$ . Lastly, M4 at low redshift exhibits super-accelerated evolution for some time but ends in the de Sitter phase.
- The jerk parameter for M1 has an approximate value of 0.79 at  $j(0)$ , M2 has an estimated value of 0.42, and M3 has an approximate value of 0.78 at  $j(0)$ . M4 has more than twice the numerical values of the  $\Lambda$ CDM model  $j(0) \approx 2.1$ .
- The snap parameter for M1, M2, and M3 predict lower values than  $\Lambda$ CDM at high redshifts, but M4 predicts higher values than  $\Lambda$ CDM. Identifying the present value of  $s$ 's parameter is a critical test. M1 predicts  $s(0) \approx -0.1$ , M2 predicts  $s(0) \approx 0.9$ , M3 predicts  $s(0) \approx 0.7$ , and M4 estimates  $s(0) \approx 0.9$ .
- The statefinder diagnostic for M1 and M4 takes values in the region  $r < 1$ ,  $s > 0$  presenting quintessence nature, then by crossing fixed  $\{r, s\} = \{1, 0\}$ ,  $\Lambda$ CDM lies in the region  $r < 1$ ,  $s < 0$  showing Chaplygin gas nature. Throughout evolution, M2 assumes values in the region  $r < 1$ ,  $s > 0$  reflect as the quintessence-like behavior. The M3 begins with values in the region  $r > 1$ ,  $s > 0$ , presenting the Chaplygin gas nature.
- The  $Om$  diagnostic for models M1 and M4 exhibit phantom region, whereas M2 & M3 is positive throughout high and low redshift, supporting a quintessence model.

Therefore, we have noticed that M2 is more viable than M1 as compared to the  $\Lambda$ CDM model, and M3 is more feasible than M2 and M4. Finally, the above four considered models are departed from the standard  $\Lambda$ CDM limit, supporting other dark energy models, and may be crucial in describing the accelerating universe.

**Acknowledgement:** AS is thankful to CSIR, Govt. of India, for providing a Senior Research Fellowship (No. 08/003(0138)/2019-EMR-I).

[1] A. G. Riess, et al., Observational evidence from supernovae for an accelerating universe and a cosmological constant, *Astron. J.* 116 (1998) 1009–1038. [arXiv:astro-ph/9805201](https://arxiv.org/abs/astro-ph/9805201), [doi:10.1086/300499](https://doi.org/10.1086/300499).

[2] S. Perlmutter, et al., Measurements of the cosmological parameters Omega and Lambda from the first 7 supernovae at  $z >= 0.35$ , *Astrophys. J.* 483 (1997) 565. [arXiv:astro-ph/9608192](https://arxiv.org/abs/astro-ph/9608192), [doi:10.1086/304265](https://doi.org/10.1086/304265).

[3] S. Perlmutter, et al., Measurements of  $\Omega$  and  $\Lambda$  from 42 high redshift supernovae, *Astrophys. J.* 517 (1999) 565–586. [arXiv:astro-ph/9812133](https://arxiv.org/abs/astro-ph/9812133), [doi:10.1086/307221](https://doi.org/10.1086/307221).

[4] D. N. Vollick, 1/R Curvature corrections as the source of the cosmological acceleration, *Phys. Rev. D* 68 (2003) 063510. [arXiv:astro-ph/0306630](https://arxiv.org/abs/astro-ph/0306630), [doi:10.1103/PhysRevD.68.063510](https://doi.org/10.1103/PhysRevD.68.063510).

[5] S. Nojiri, S. D. Odintsov, Modified gravity with negative and positive powers of the curvature: Unification of the inflation and of the cosmic acceleration, *Phys. Rev. D* 68 (2003) 123512. [arXiv:hep-th/0307288](https://arxiv.org/abs/hep-th/0307288), [doi:10.1103/PhysRevD.68.123512](https://doi.org/10.1103/PhysRevD.68.123512).

[6] J. L. Tonry, et al., Cosmological results from high- $z$  supernovae, *Astrophys. J.* 594 (2003) 1–24. [arXiv:astro-ph/0305008](https://arxiv.org/abs/astro-ph/0305008), [doi:10.1086/376865](https://doi.org/10.1086/376865).

[7] A. G. Riess, et al., Type Ia supernova discoveries at  $z > 1$  from the Hubble Space Telescope: Evidence for past deceleration and constraints on dark energy evolution, *Astrophys. J.* 607 (2004) 665–687. [arXiv:astro-ph/0402512](https://arxiv.org/abs/astro-ph/0402512), [doi:10.1086/383612](https://doi.org/10.1086/383612).

[8] A. Clocchiatti, et al., Hubble Space Telescope and Ground-Based Observations of Type Ia Supernovae at Redshift 0.5: Cosmological Implications, *Astrophys. J.* 642 (2006) 1–21. [arXiv:astro-ph/0510155](https://arxiv.org/abs/astro-ph/0510155), [doi:10.1086/498491](https://doi.org/10.1086/498491).

[9] R. R. Caldwell, W. Komp, L. Parker, D. A. T. Vanzella, A Sudden gravitational transition, *Phys. Rev. D* 73 (2006) 023513. [arXiv:astro-ph/0507622](https://arxiv.org/abs/astro-ph/0507622), [doi:10.1103/PhysRevD.73.023513](https://doi.org/10.1103/PhysRevD.73.023513).

[10] V. Sahni, A. A. Starobinsky, The Case for a positive cosmological Lambda term, *Int. J. Mod. Phys. D* 9 (2000) 373–444. [arXiv:astro-ph/9904398](https://arxiv.org/abs/astro-ph/9904398), [doi:10.1142/S0218271800000542](https://doi.org/10.1142/S0218271800000542).

[11] T. Padmanabhan, Cosmological constant: The Weight of the vacuum, *Phys. Rept.* 380 (2003) 235–320. [arXiv:hep-th/0212290](https://arxiv.org/abs/hep-th/0212290), [doi:10.1016/S0370-1573\(03\)00120-0](https://doi.org/10.1016/S0370-1573(03)00120-0).

[12] P. J. E. Peebles, B. Ratra, The Cosmological Constant and Dark Energy, *Rev. Mod. Phys.* 75 (2003) 559–606. [arXiv:astro-ph/0207347](https://arxiv.org/abs/astro-ph/0207347), [doi:10.1103/RevModPhys.75.559](https://doi.org/10.1103/RevModPhys.75.559).

[13] E. J. Copeland, M. Sami, S. Tsujikawa, Dynamics of dark energy, *International Journal of Modern Physics D* 15 (11) (2006) 1753–1935.

[14] L. Amendola, S. Tsujikawa, Dark energy: theory and observations, Cambridge University Press, 2010.

[15] P. J. Steinhardt, L. Wang, I. Zlatev, Cosmological tracking solutions, *Physical Review D* 59 (12) (1999) 123504.

[16] S. Weinberg, The Cosmological Constant Problem, *Rev. Mod. Phys.* 61 (1989) 1–23. [doi:10.1103/RevModPhys.61.1](https://doi.org/10.1103/RevModPhys.61.1).

[17] S. Capozziello, V. F. Cardone, E. Elizalde, S. Nojiri, S. D. Odintsov, Observational constraints on dark energy with generalized equations of state, *Phys. Rev. D* 73 (2006) 043512. [arXiv:astro-ph/0508350](https://arxiv.org/abs/astro-ph/0508350), [doi:10.1103/PhysRevD.73.043512](https://doi.org/10.1103/PhysRevD.73.043512).

[18] C. Escamilla-Rivera, S. Capozziello, Unveiling cosmography from the dark energy equation of state, *Int. J. Mod. Phys. D* 28 (12) (2019) 1950154. [arXiv:1905.04602](https://arxiv.org/abs/1905.04602), [doi:10.1142/S0218271819501542](https://doi.org/10.1142/S0218271819501542).

[19] U. Debnath, Gravitational waves for variable modified Chaplygin gas and some parametrizations of dark energy in the background of FRW universe, *Eur. Phys. J. Plus* 135 (2) (2020) 135. [doi:10.1140/epjp/s13360-020-00219-9](https://doi.org/10.1140/epjp/s13360-020-00219-9).

[20] S. del Campo, I. Duran, R. Herrera, D. Pavon, Three thermodynamically-based parameterizations of the deceleration parameter, *Phys. Rev. D* 86 (2012) 083509. [arXiv:1209.3415](https://arxiv.org/abs/1209.3415), [doi:10.1103/PhysRevD.86.083509](https://doi.org/10.1103/PhysRevD.86.083509).

[21] J. Cunha, J. A. S. d. Lima, Transition redshift: new kinematic constraints from supernovae, *Monthly Notices of the Royal Astronomical Society* 390 (1) (2008) 210–217.

[22] J. V. Cunha, Kinematic Constraints to the Transition Redshift from SNe Ia Union Data, *Phys. Rev. D* 79 (2009) 047301. [arXiv:0811.2379](https://arxiv.org/abs/0811.2379), [doi:10.1103/PhysRevD.79.047301](https://doi.org/10.1103/PhysRevD.79.047301).

[23] A. G. Riess, et al., Type Ia supernova discoveries at  $z > 1$  from the Hubble Space Telescope: Evidence for past deceleration and constraints on dark energy evolution, *Astrophys. J.* 607 (2004) 665–687. [arXiv:astro-ph/0402512](https://arxiv.org/abs/astro-ph/0402512), [doi:10.1086/383612](https://doi.org/10.1086/383612).

[24] L.-I. Xu, C.-W. Zhang, B.-R. Chang, H.-Y. Liu, Constraints to deceleration parameters by recent cosmic observations, *Mod. Phys. Lett. A* 23 (2008) 1939–1948. [arXiv:astro-ph/0701519](https://arxiv.org/abs/astro-ph/0701519), [doi:10.1142/S0217732308025991](https://doi.org/10.1142/S0217732308025991).

[25] L. Xu, J. Lu, Cosmic constraints on deceleration parameter with SNe Ia and CMB, *Mod. Phys. Lett. A* 24 (2009) 369–376. [doi:10.1142/S0217732309027212](https://arxiv.org/abs/10.1142/S0217732309027212).

[26] R. Nair, S. Jhingan, D. Jain, Cosmokinetics: a joint analysis of standard candles, rulers and cosmic clocks, *Journal of Cosmology and Astroparticle Physics* 2012 (01) (2012) 018.

[27] O. Akarsu, T. Dereli, S. Kumar, L. Xu, Probing kinematics and fate of the Universe with linearly time-varying deceleration parameter, *Eur. Phys. J. Plus* 129 (2014) 22. [arXiv:1305.5190](https://arxiv.org/abs/1305.5190), [doi:10.1140/epjp/i2014-14022-6](https://doi.org/10.1140/epjp/i2014-14022-6).

[28] B. Santos, J. C. Carvalho, J. S. Alcaniz, Current constraints on the epoch of cosmic acceleration, *Astroparticle Physics* 35 (1) (2011) 17–20.

[29] Y.-G. Gong, A. Wang, Reconstruction of the deceleration parameter and the equation of state of dark energy, *Phys. Rev. D* 75 (2007) 043520. [arXiv:astro-ph/0612196](https://arxiv.org/abs/astro-ph/0612196), [doi:10.1103/PhysRevD.75.043520](https://doi.org/10.1103/PhysRevD.75.043520).

[30] M. S. Turner, A. G. Riess, Do SNe Ia provide direct evidence for past deceleration of the universe?, *Astrophys. J.* 569 (2002) 18. [arXiv:astro-ph/0106051](https://arxiv.org/abs/astro-ph/0106051), [doi:10.1086/338580](https://doi.org/10.1086/338580).

[31] A. Al Mamon, S. Das, A divergence free parametrization of deceleration parameter for scalar field dark energy, *Int. J. Mod. Phys. D* 25 (03) (2016) 1650032. [arXiv:1507.00531](https://arxiv.org/abs/1507.00531), [doi:10.1142/S0218271816500322](https://doi.org/10.1142/S0218271816500322).

[32] G. N. Gadbial, S. Mandal, P. K. Sahoo, Parametrization

of deceleration parameter in  $f(q)$  gravity, *Physics* 4 (4) (2022) 1403–1412.

[33] A. Bouali, B. Shukla, H. Chaudhary, R. K. Tiwari, M. Samar, G. Mustafa, Cosmological tests of parametrization  $q = \alpha - \beta h$  in  $f(q)$  flrw cosmology, *International Journal of Geometric Methods in Modern Physics* (2023).

[34] A. Bouali, H. Chaudhary, A. Mehrotra, S. Pacif, Model-independent study for a quintessence model of dark energy: Analysis and observational constraints, arXiv preprint arXiv:2304.02652 (2023).

[35] A. A. Mamon, S. Das, A parametric reconstruction of the deceleration parameter, *The European Physical Journal C* 77 (7) (2017) 495.

[36] A. Bouali, H. Chaudhary, U. Debnath, T. Roy, G. Mustafa, Constraints on the Parameterized Deceleration Parameter in FRW Universe (1 2023). [arXiv:2301.12107](https://arxiv.org/abs/2301.12107).

[37] S. Capozziello, R. D'Agostino, O. Luongo, Thermodynamic parametrization of dark energy, *Phys. Dark Univ.* 36 (2022) 101045. [arXiv:2202.03300](https://arxiv.org/abs/2202.03300), [doi:10.1016/j.dark.2022.101045](https://doi.org/10.1016/j.dark.2022.101045).

[38] U. Alam, V. Sahni, T. D. Saini, A. A. Starobinsky, Is there supernova evidence for dark energy metamorphosis ?, *Mon. Not. Roy. Astron. Soc.* 354 (2004) 275. [arXiv:astro-ph/0311364](https://arxiv.org/abs/astro-ph/0311364), [doi:10.1111/j.1365-2966.2004.08189.x](https://doi.org/10.1111/j.1365-2966.2004.08189.x).

[39] U. Alam, V. Sahni, A. A. Starobinsky, The case for dynamical dark energy revisited, *Journal of Cosmology and Astroparticle Physics* 2004 (06) (2004) 008.

[40] T. Bandyopadhyay, U. Debnath, Fluid accretion upon higher-dimensional wormhole and black hole for parameterized deceleration parameter, *International Journal of Geometric Methods in Modern Physics* 19 (12) (2022) 2250182.

[41] R. Kundu, U. Debnath, A. Pradhan, Studying the optical depth behaviour of parametrized deceleration parameter in non-flat universe, *International Journal of Geometric Methods in Modern Physics* (2023).

[42] H. Padé, Sur la représentation approchée d'une fonction par des fractions rationnelles, in: *Annales scientifiques de l'Ecole normale supérieure*, Vol. 9, 1892, pp. 3–93.

[43] H. Wei, X.-P. Yan, Y.-N. Zhou, Cosmological applications of pade approximant, *Journal of Cosmology and Astroparticle Physics* 2014 (01) (2014) 045.

[44] M. Rezaei, M. Malekjani, S. Basilakos, A. Mehrabi, D. F. Mota, Constraints to dark energy using pade parameterizations, *The Astrophysical Journal* 843 (1) (2017) 65.

[45] D. Foreman-Mackey, D. W. Hogg, D. Lang, J. Goodman, emcee: the mcmc hammer, *Publications of the Astronomical Society of the Pacific* 125 (925) (2013) 306.

[46] W. Handley, M. Hobson, A. Lasenby, Polychord: nested sampling for cosmology, *Monthly Notices of the Royal Astronomical Society: Letters* 450 (1) (2015) L61–L65.

[47] A. Lewis, Getdist: a python package for analysing monte carlo samples, arXiv preprint arXiv:1910.13970 (2019).

[48] E. Gaztanaga, C. Bonvin, L. Hui, Measurement of the dipole in the cross-correlation function of galaxies, *Journal of Cosmology and Astroparticle Physics* 2017 (01) (2017) 032.

[49] A. Bouali, H. Chaudhary, R. Hama, T. Harko, S. V. Sabau, M. S. Martín, Cosmological tests of the osculating barthel-kropina dark energy model, *The European Physical Journal C* 83 (2) (2023) 121.

[50] M. Kowalski, D. Rubin, G. Aldering, R. Agostinho, A. Amadon, R. Amanullah, C. Balland, K. Barbary, G. Blanc, P. Challis, et al., Improved cosmological constraints from new, old, and combined supernova data sets, *The Astrophysical Journal* 686 (2) (2008) 749.

[51] R. Amanullah, C. Lidman, D. Rubin, G. Aldering, P. Astier, K. Barbary, M. Burns, A. Conley, K. Dawson, S. Deustua, et al., Spectra and hubble space telescope light curves of six type ia supernovae at  $0.511 < z < 1.12$  and the union2 compilation, *The Astrophysical Journal* 716 (1) (2010) 712.

[52] N. Suzuki, D. Rubin, C. Lidman, G. Aldering, R. Amanullah, K. Barbary, L. Barrientos, J. Botyanszki, M. Brodin, N. Connolly, et al., The hubble space telescope cluster supernova survey. v. improving the dark-energy constraints above  $z > 1$  and building an early-type-hosted supernova sample, *The Astrophysical Journal* 746 (1) (2012) 85.

[53] M. Betoule, R. Kessler, J. Guy, J. Mosher, D. Hardin, R. Biswas, P. Astier, P. El-Hage, M. Konig, S. Kuhlmann, et al., Improved cosmological constraints from a joint analysis of the sdss-ii and snls supernova samples, *Astronomy & Astrophysics* 568 (2014) A22.

[54] D. M. Scolnic, D. Jones, A. Rest, Y. Pan, R. Chornock, R. Foley, M. Huber, R. Kessler, G. Narayan, A. Riess, et al., The complete light-curve sample of spectroscopically confirmed sne ia from pan-starrs1 and cosmological constraints from the combined pantheon sample, *The Astrophysical Journal* 859 (2) (2018) 101.

[55] D. Scolnic, D. Brout, A. Carr, A. G. Riess, T. M. Davis, A. Dwomoh, D. O. Jones, N. Ali, P. Charvú, R. Chen, et al., The pantheon+ type ia supernova sample: the full dataset and light-curve release, arXiv preprint arXiv:2112.03863 (2021).

[56] D. Benisty, D. Staicova, Testing late-time cosmic acceleration with uncorrelated baryon acoustic oscillation dataset, *Astronomy & Astrophysics* 647 (2021) A38.

[57] W. J. Percival, B. A. Reid, D. J. Eisenstein, N. A. Bahcall, T. Budavari, J. A. Frieman, M. Fukugita, J. E. Gunn, Ž. Ivezić, G. R. Knapp, et al., Baryon acoustic oscillations in the Sloan digital sky survey data release 7 galaxy sample, *Monthly Notices of the Royal Astronomical Society* 401 (4) (2010) 2148–2168.

[58] F. Beutler, C. Blake, M. Colless, D. H. Jones, L. Staveley-Smith, L. Campbell, Q. Parker, W. Saunders, F. Watson, The 6df galaxy survey: baryon acoustic oscillations and the local hubble constant, *Monthly Notices of the Royal Astronomical Society* 416 (4) (2011) 3017–3032.

[59] T. Delubac, J. Rich, S. Bailey, A. Font-Ribera, D. Kirkby, J.-M. Le Goff, M. M. Pieri, A. Slosar, É. Aubourg, J. E. Bautista, et al., Baryon acoustic oscillations in the ly $\alpha$  forest of boss quasars, *Astronomy & Astrophysics* 552 (2013) A96.

[60] L. Anderson, E. Aubourg, S. Bailey, D. Bizyaev, M. Blanton, A. S. Bolton, J. Brinkmann, J. R. Brownstein, A. Burden, A. J. Cuesta, et al., The clustering of galaxies in the sdss-iii baryon oscillation spectroscopic survey: baryon acoustic oscillations in the data release 9 spectroscopic galaxy sample, *Monthly Notices of the Royal Astronomical Society* 427 (4) (2012) 3435–3467.

[61] H.-J. Seo, S. Ho, M. White, A. J. Cuesta, A. J. Ross, S. Saito, B. Reid, N. Padmanabhan, W. J. Percival, R. De Putter, et al., Acoustic scale from the angular

power spectra of sdss-iii dr8 photometric luminous galaxies, *The Astrophysical Journal* 761 (1) (2012) 13.

[62] A. J. Ross, L. Samushia, C. Howlett, W. J. Percival, A. Burden, M. Manera, The clustering of the sdss dr7 main galaxy sample–i. a 4 per cent distance measure at  $z=0.15$ , *Monthly Notices of the Royal Astronomical Society* 449 (1) (2015) 835–847.

[63] R. Tojeiro, A. J. Ross, A. Burden, L. Samushia, M. Manera, W. J. Percival, F. Beutler, J. Brinkmann, J. R. Brownstein, A. J. Cuesta, et al., The clustering of galaxies in the sdss-iii baryon oscillation spectroscopic survey: galaxy clustering measurements in the low-redshift sample of data release 11, *Monthly Notices of the Royal Astronomical Society* 440 (3) (2014) 2222–2237.

[64] J. E. Bautista, M. Vargas-Magaña, K. S. Dawson, W. J. Percival, J. Brinkmann, J. Brownstein, B. Camacho, J. Comparat, H. Gil-Marín, E.-M. Mueller, et al., The sdss-iv extended baryon oscillation spectroscopic survey: baryon acoustic oscillations at redshift of 0.72 with the dr14 luminous red galaxy sample, *The Astrophysical Journal* 863 (1) (2018) 110.

[65] E. De Carvalho, A. Bernui, G. Carvalho, C. Novaes, H. Xavier, Angular baryon acoustic oscillation measure at  $z=2.225$  from the sdss quasar survey, *Journal of Cosmology and Astroparticle Physics* 2018 (04) (2018) 064.

[66] M. Ata, F. Baumgarten, J. Bautista, F. Beutler, D. Bizyaev, M. R. Blanton, J. A. Blazek, A. S. Bolton, J. Brinkmann, J. R. Brownstein, et al., The clustering of the sdss-iv extended baryon oscillation spectroscopic survey dr14 quasar sample: first measurement of baryon acoustic oscillations between redshift 0.8 and 2.2, *Monthly Notices of the Royal Astronomical Society* 473 (4) (2018) 4773–4794.

[67] T. Abbott, F. Abdalla, A. Alarcon, S. Allam, F. Andrade-Oliveira, J. Annis, S. Avila, M. Banerji, N. Banik, K. Bechtol, et al., Dark energy survey year 1 results: Measurement of the baryon acoustic oscillation scale in the distribution of galaxies to redshift 1, *Monthly Notices of the Royal Astronomical Society* 483 (4) (2019) 4866–4883.

[68] Z. Molavi, A. Khodam-Mohammadi, Observational tests of gauss-bonnet like dark energy model, *The European Physical Journal Plus* 134 (6) (2019) 254.

[69] N. B. Hogg, M. Martinelli, S. Nesseris, Constraints on the distance duality relation with standard sirens, *Journal of Cosmology and Astroparticle Physics* 2020 (12) (2020) 019.

[70] M. Martinelli, C. J. A. P. Martins, S. Nesseris, D. Sapone, I. Tutusaus, A. Avgoustidis, S. Camera, C. Carbone, S. Casas, S. Ilić, et al., Euclid: Forecast constraints on the cosmic distance duality relation with complementary external probes, *Astronomy & Astrophysics* 644 (2020) A80.

[71] L. Chen, Q.-G. Huang, K. Wang, Distance priors from planck final release, *Journal of Cosmology and Astroparticle Physics* 2019 (02) (2019) 028.

[72] M. Shahalam, S. Sami, A. Agarwal, Om diagnostic applied to scalar field models and slowing down of cosmic acceleration, *Monthly Notices of the Royal Astronomical Society* 448 (3) (2015) 2948–2959.

[73] V. Sahni, T. D. Saini, A. A. Starobinsky, U. Alam, Statefinder—a new geometrical diagnostic of dark energy, *Journal of Experimental and Theoretical Physics Letters* 77 (2003) 201–206.

[74] U. Alam, V. Sahni, T. Deep Saini, A. Starobinsky, Exploring the expanding universe and dark energy using the statefinder diagnostic, *Monthly Notices of the Royal Astronomical Society* 344 (4) (2003) 1057–1074.

[75] M. Sami, M. Shahalam, M. Skugoreva, A. Toporensky, Cosmological dynamics of a nonminimally coupled scalar field system and its late time cosmic relevance, *Physical Review D* 86 (10) (2012) 103532.

[76] R. Myrzakulov, M. Shahalam, Statefinder hierarchy of bimetric and galileon models for concordance cosmology, *Journal of Cosmology and Astroparticle Physics* 2013 (10) (2013) 047.

[77] V. Sahni, T. D. Saini, A. A. Starobinsky, U. Alam, Statefinder: A New geometrical diagnostic of dark energy, *JETP Lett.* 77 (2003) 201–206. [arXiv:astro-ph/0201498](https://arxiv.org/abs/astro-ph/0201498), doi:10.1134/1.1574831.

[78] V. Sahni, A. Shafieloo, A. A. Starobinsky, Two new diagnostics of dark energy, *Phys. Rev. D* 78 (2008) 103502. [arXiv:0807.3548](https://arxiv.org/abs/0807.3548), doi:10.1103/PhysRevD.78.103502.

[79] V. Sahni, A. Shafieloo, A. A. Starobinsky, Two new diagnostics of dark energy, *Physical Review D* 78 (10) (2008) 103502.

[80] C. Zunckel, C. Clarkson, Consistency tests for the cosmological constant, *Physical Review Letters* 101 (18) (2008) 181301.

[81] M. Shahalam, S. Pathak, M. Verma, M. Y. Khlopov, R. Myrzakulov, Dynamics of interacting quintessence, *The European Physical Journal C* 75 (2015) 1–9.

[82] A. Agarwal, R. Myrzakulov, S. Pacif, M. Shahalam, Cosmic acceleration from coupling of baryonic and dark matter components: Analysis and diagnostics, *International Journal of Modern Physics D* 28 (06) (2019) 1950083.

[83] A. Jawad, S. Qummer, S. Rani, M. Younas, Generalized interaction term inspired dark energy model in fractal universe, *Mod. Phys. Lett. A* 35 (15) (2020) 2050126. doi:10.1142/S0217732320501266.

[84] A. Khodam-Mohammadi, M. Malekjani, Interacting entropy-corrected holographic scalar field models in non-flat universe, *Commun. Theor. Phys.* 55 (2011) 942–948. [arXiv:1004.1720](https://arxiv.org/abs/1004.1720), doi:10.1088/0253-6102/55/5/37.

[85] M. Malekjani, A. Khodam-Mohammadi, Statefinder diagnosis and the interacting ghost model of dark energy, *Astrophys. Space Sci.* 343 (2013) 451–461. [arXiv:1202.4154](https://arxiv.org/abs/1202.4154), doi:10.1007/s10509-012-1230-3.

[86] M. Malekjani, A. Khodam-Mohammadi, N. Nazari-pooya, Cosmological evolution and statefinder diagnostic for new holographic dark energy model in non flat universe, *Astrophys. Space Sci.* 332 (2011) 515–524. [arXiv:1011.4805](https://arxiv.org/abs/1011.4805), doi:10.1007/s10509-010-0550-4.

[87] M. Jamil, D. Momeni, R. Myrzakulov, Observational constraints on non-minimally coupled galileon model, *The European Physical Journal C* 73 (3) (2013) 2347.

[88] P. De Fromont, C. De Rham, L. Heisenberg, A. Matas, Superluminality in the bi-and multi-galileon, *Journal of High Energy Physics* 2013 (7) (2013) 1–29.

[89] H. Akaike, A new look at the statistical model identification, *IEEE transactions on automatic control* 19 (6) (1974) 716–723.

[90] M. Li, X. Li, X. Zhang, Comparison of dark energy models: A perspective from the latest observational data, *Science China Physics, Mechanics and Astronomy* 53 (9) (2010) 1631–1645.

[91] K. Burnham, D. R. Anderson, *Model selection and multimodel inference*, New York: Springer (2002).

- [92] K. P. Burnham, D. R. Anderson, Multimodel inference: understanding aic and bic in model selection, *Sociological methods & research* 33 (2) (2004) 261–304.
- [93] A. R. Liddle, Information criteria for astrophysical model selection, *Monthly Notices of the Royal Astronomical Society: Letters* 377 (1) (2007) L74–L78.